ANNALS OF PHYSICS 197, 205–264 (1990)

A Density Variational Approach to Nuclear Giant Resonances at Zero and Finite Temperature*

P. GLEISSL AND M. BRACK

Niels Bohr Institutet, Blegdamsvej 17, DK-2100 Copenhagen, Denmark and Institut für Theoretische Physik, Universität Regensburg, D-8400 Regensburg, West Germany†

J. MEYER

Institut de Physique Nucléaire (et IN2P3), Université de Lyon-I, F-69622, Villeurbanne, France

AND

P. QUENTIN

Laboratoire de Physique Théorique,‡ Université de Bordeaux-I, F-33170 Gradignan, France

Received January 25, 1989

We present a density functional approach to the description of nuclear giant resonances (GR), using Skyrme type effective interactions. We exploit hereby the theorems of Thouless and others, relating RPA sum rules to static (constrained) Hartree–Fock expectation values. The latter are calculated both microscopically and, where shell effects are small enough to allow it, semiclassically by a density variational method employing the gradient-expanded density functionals of the extended Thomas–Fermi model. In contrast to the widely spread fluid-dynamical approach, our method has the advantage of dealing with realistic density profiles with continuous surfaces and of allowing us to use realistic effective nuclear interactions including nonlocalities, such as effective mass and spin-orbit terms and the Coulomb interaction. We obtain an excellent overall description of both systematics and detailed isotopic dependence of GR energies, in particular with the Skyrme force SkM*. For the breathing modes (isoscalar and isovector giant monopole modes), and to some extent also for the isovector dipole mode, the A-dependence of the experimental peak energies is better described by coupling two different modes (corresponding to two different excitation operators) of the same spin and parity and evaluating the eigenmodes of the coupled system. Our calculations are also extended to hot nuclei (without angular momentum) and the temperature dependence of the various GR energies is discussed.

* Work partially supported by the French–German Scientific Exchange Program "PROCOPE."

† Permanent address.

‡ Unité associée au C.N.R.S.

0003-4916/90 $7.50

CONTENTS

1. INTRODUCTION

The existence of strong resonances in nuclear photo-absorption cross sections, established in 1947 by Baldwin and Klaiber [1], has been theoretically explained [2, 3] as the manifestation of a collective motion of the nucleus of isovector dipole type [4]. Later on, other excitations of various multipolarities with strongly collective character, both of isoscalar and isovector nature, have been observed [5]. They are all understood in terms of small-amplitude vibrations as a response of the nucleus to an external field generated by electromagnetic or hadronic probes.

A relevant microscopic description of such quantal harmonic modes is found in selfconsistent RPA calculations where both the single-particles states in the mean field corresponding to the nuclear ground state and the particle–hole interaction responsible for the excitation are stemming from the same effective nucleon–nucleon force. Such calculations are tractable but somewhat complicated and time consuming for large-scale investigations. An elegant bypass is provided [6] by the sum rule approach to the strength function $S_Q(E)$ associated with a given excitation operator $\hat{Q}$. In general terms, the sum rule m_k expresses the kth moment (in energy E) of the strength distribution $S_Q(E)$ in a compact form involving only the properties (i.e., the wavefunction) of the ground state. Furthermore, upon restricting the summations involved in such moments to RPA states only, theorems have been proven [7–9] which allow to obtain some of the moments m_k merely from the knowledge of the uncorrelated Hartree–Fock (HF) ground state wavefunction.

In the present paper we will make use of these sum rules to describe nuclear giant resonances, hereby replacing the static microscopic HF treatment of the nuclear ground state by a selfconsistent semiclassical density variational approach using the extended Thomas–Fermi (ETF) functionals [10]. In this approach, average quantal effects due to the finite size and the surface diffuseness of the nucleus are included in the form of density gradient corrections, but the shell effects due to the inhomogeneous distribution of the single-particle energies are explicitly omitted. For monopole and dipole giant resonances this seems, in fact, to be justified by their successfull description in terms of classical hydrodynamics [11, 12]. However, how possibly accidental this success is, may be illustrated by the failure of

hydrodynamics to describe correctly the A-dependence of the isoscalar giant quadrupole resonance energies. The latter has been correctly reproduced by simple but microscopical approaches [13–18]. It has also been retrieved in a classical framework by the so-called fluid-dynamical approach [19–23] whose main ingredient is the dynamical distortion of the Fermi sphere in momentum space. This leads to the explanation of the giant quadrupole mode (and various other modes) as excitations of Landau zero-sound type [24]. The distortion of the Fermi sphere in momentum space is intimately related to the scaling behaviour of the quantal single-particle wavefunctions in coordinate space. Both mechanisms affect the restoring forces in the same way [25, 26]. Through the use of sum rules it is, indeed, possible to incorporate these effects in the semiclassical density variational approach described in this paper. We should, however, stress the absolute necessity of building in these single-particle effects *before* making semiclassical approximations, as will be discussed in more detail in Section 2.3.

With the noticeable exception of the electric dipole photo-absorption process, the radial dependence of the excitation operator leading to a given giant resonance is generally not very well known. Therefore, one first has to make a reasonable guess for it. Moreover, even having made this choice, one still has to decide—whenever dealing with a substitute for a fully microscopic RPA calculation—on the deformation path along which the collective motion will take place. This latter choice specifies, in fact, the energy range in which one will explore the strength distribution for the chosen collective operator. For instance, for fast diabatic motion dominating the higher energy region of isoscalar giant resonances, the relevant collective path is that of a generalized scaling type leading to the positive energy-weighted m_1 and m_3 sum rules [6]. A prototype of this kind of dynamics appears to be the high-lying giant quadrupole resonance. A particular realisation of the scaling approach to this mode due to Tassie [27] is, indeed, fully consistent with the results of microscopic approaches for the transition density (see, e.g., Ref. [28]). Also for the monopole mode, a similar agreement between the scaling ansatz [29] and RPA results [30] has been found. (For the isovector dipole mode, the scaling approach corresponds to an almost pure surface mode and is not sufficient to explain the experimental data; it must be supplemented [12, 31] by some amount of volume oscillations with a fixed surface [4].) On the other hand, for slow collective motion (adiabatic in a restricted acception) prevailing in the low-energy domain, one would rather consider a collective path generated by constrained HF calculations leading to the knowledge of the negative energy-weighted m_{-1} and m_{-3} sum rules [6, 32, 33]. Apart from the particular situations where the Pauli principle hinders low-lying excitation strength (as in light closed-shell nuclei; see, e.g., the calculations [34] for ^{16}O and ^{40}Ca), such collective paths are tailored for the description of low-lying surface vibrations rather than for giant resonances.

During the last few years, an increased interest has been raised in giant resonances built not on the ground state configuration but on top of excited nuclear states, as suggested years ago by Brink [35]. Indeed, recent experimental analyses of gamma ray spectra observed in (*heavy-ion*, $xn\,\gamma$) [36] and in (p, γ) reactions [37]

give evidence for the existence of isovector dipole giant resonances built on highly excited compound nuclei. The extraction of resonance parameters from such data is a complicated task, in particular, for the heavy-ion reactions in view of the coupling of the vibration mode with the rotational motion of possible deformed excited states [38].

As a first theoretical approach it is natural to extend the study of vibrational modes to excited nuclei described as grand-canonical equilibrium states at a given temperature [39, 40]. The corresponding microscopical framework is the finite-temperature HF + RPA approach [41]. Selfconsistent calculations along these lines have recently been performed [42–45]. Similarly to the zero-temperature case, a finite-temperature sum-rule approach has also been proposed [46–50]. Since shell effects are known [39, 51] to disappear above nuclear temperatures[1] $T \gtrsim 2$–3 MeV, purely semiclassical methods apply particularly well at such temperatures. Recently, the ETF density functionals [10] have been rigorously generalized for fermion systems at finite temperatures [52–54] and the corresponding variational calculations have been shown [10, 52, 54] to yield the same results as HF calculations for $T \gtrsim 2.5$–3 MeV. We shall therefore in the present paper extend our numerical studies of nuclear giant resonances systematically to modes involving statistically equilibrated "hot" nuclear systems.

In our calculations we employ throughout the Skyrme effective nucleon–nucleon interaction [55, 56] in its generalized form (see, e.g., Ref. [34]). (The details of the Skyrme force and the parameter sets used in this article are given in Appendix 2.1.) In most of the present results we have used the parametrisation SkM* obtained from a fit to radii and binding energies of spherical nuclei and the fission barriers of heavy actinide nuclei [10, 57]. This force is believed to yield not only good ground state properties for nuclei not too far away from the β-stability line, but also reasonable surface and deformation properties. It has the same nuclear matter properties as the force SkM previously determined [58] from a fit to isoscalar monopole and quadrupole giant resonances; in particular, its incompressibility modulus $K_\infty = 217$ MeV is low enough to give the correct breathing mode energies. We neglect throughout the pairing correlations which—besides doubly closed-shell nuclei where they are negligible anyhow—generally give very small corrections to the giant resonance properties, as seen, e.g., in the isovector dipole case [31].

The present work deals mainly with natural-parity electric modes. Indeed, the Skyrme force parametrisations available so far—apart from rather special sets tailored to the reproduction of pairing properties [59] or some magnetic giant resonances [60]—do not yield fully satisfactory results in all channels including the spin and spin–isospin degrees of freedom. Of course, extensions of our studies to the magnetic modes would provide a much needed help in the timely task of fitting the parameters x_1 and x_2 (i.e., the finite-range exchange terms) governing these modes.

We shall mainly concentrate our semiclassical calculations on the positive energy

[1] Throughout this paper, we put the Boltzmann constant $k = 1$ and use energy units (MeV) for the temperature.

weighted sum rules m_3 and m_1, where the shell effects are minimal even at zero temperature. To investigate the role of the shell effects in negative energy weighted sum rules m_{-1} and m_{-3}, we shall also report on the corresponding HF calculations and compare them to the density variational results.

The paper is organized as follows. Section 2 presents the general theoretical framework of our studies. For the sake of a clear presentation, we have collected most of the formulae in the Appendix. In Section 3 we shall successively report our results on the monopole, dipole, quadrupole, and octupole modes at zero temperature and finally discuss the temperature dependence of the giant resonance energies and sum rules. The final Section 4 is, as usual, devoted to a summary and conclusions.

2. Survey of the Theoretical Framework

2.1. *Sum Rules, Excitation Operators, and Collective Variables*

To characterize the response of a nucleus to an excitation operator $\hat{Q}$, one defines the associated strength function $S_Q(E)$ as

$$S_Q(E) = \sum_{n \neq 0} |\langle n| \hat{Q} |0\rangle|^2 \, \delta(E - E_n), \tag{2.1}$$

where E_n, $|n\rangle$ are the exact eigensolutions of the total nuclear Hamiltonian $\hat{H} = \hat{T} + \hat{V}$, and $E_0 = 0$, $|0\rangle$ correspond to the ground state. Practically one often knows only some moments of this function

$$m_k(\hat{Q}) = \int_0^\infty E^k S_Q(E) \, dE = \sum_{n \neq 0} E_n^k \, |\langle n| \hat{Q} |0\rangle|^2. \tag{2.2}$$

The interest of such moments lies in the fact that for positive integer k they can be evaluated as expectation values in the exact ground state $|0\rangle$ of some operators. In particular, one has

$$m_1(\hat{Q}) = \tfrac{1}{2}\langle 0| \, [\hat{Q}, [\hat{H}, \hat{Q}]] \, |0\rangle, \tag{2.3a}$$

$$m_3(\hat{Q}) = \tfrac{1}{2}\langle 0| \, [[[\hat{H}, \hat{Q}], [\hat{H}, [\hat{Q}, \hat{H}]]] \, |0\rangle. \tag{2.3b}$$

The moment m_{-1} in turn is half the ground-state polarisability α with respect to the operator $\hat{Q}$:

$$m_{-1}(\hat{Q}) = \frac{1}{2} \alpha(\hat{Q}) = \frac{1}{2} \frac{d}{d\lambda} \langle \lambda| \hat{Q} |\lambda\rangle \Big|_{\lambda = 0} = \frac{1}{2} \frac{d^2}{d\lambda^2} \langle \lambda| \hat{H} |\lambda\rangle \Big|_{\lambda = 0}, \tag{2.4}$$

where $|\lambda\rangle$ is the ground state of the "constrained" Hamiltonian $\hat{H} - \lambda \hat{Q}$.

The sum rules in Eqs. (2.3), (2.4) so far have little practical value since they involve the unknown exact ground state wavefunctions. Some particularly interest-

ing approximations arise when the exact eigensolutions in Eq. (2.1) are replaced by RPA solutions. Then it is possible to show [7–9] that the sum rules in Eqs. (2.3), (2.4) are exactly obtained replacing the RPA ground state by the uncorrelated HF or constrained HF (CHF) ground state. Similarly, starting from the RPA approximation (2.1) to $S_Q(E)$ it can be shown [32, 33] that the moment $m_{-3}(\hat{Q})$ is a polarisability with respect to the time-odd (cranking) operator $\hat{P}$ classically conjugated to $\hat{Q}$ in the adiabatic limit of the TDHF framework [61, 62],

$$m_{-3}(\hat{Q}) = \frac{1}{2\hbar^2} \frac{\partial}{\partial \mu} \langle \lambda\mu | \hat{P} | \lambda\mu \rangle \Big|_{\mu=\lambda=0}, \tag{2.5}$$

where

$$\hat{P} = i\hbar \left[\frac{\partial \rho(\lambda)}{\partial \lambda}, \rho(\lambda) \right] \tag{2.6}$$

and $\rho(\lambda)$ is the one-body density matrix associated to the slater determinant $|\lambda\rangle$. In Eq. (2.5), $|\lambda\mu\rangle$ is the ground state solution of the operator $\hat{H} - \lambda\hat{Q} - \mu\hat{P}$. Practically, m_{-3} is most easily evaluated by making use of the relation (see, e.g., Ref. [62])

$$M(Q) = \frac{\hbar^2}{2} \frac{m_{-3}(\hat{Q})}{[m_{-1}(\hat{Q})]^2}, \tag{2.7}$$

where $M(Q)$ is the adiabatic mass parameter associated to the collective variable $Q = \langle \hat{Q} \rangle$ in the adiabatic TDHF approach using a CHF collective path. As to the polarisability $m_{-1}(\hat{Q})$, it can either be obtained directly through Eq. (2.4) or by determining numerically (e.g., by a three-point method) the stiffness parameter C of the corresponding CHF deformation energy curve $E_{\mathrm{HF}}(Q)$ at the ground state with $m_{-1}(\hat{Q}) = 1/(2C)$. A comparison of the values obtained by the two approaches provides an estimate of the validity of the underlying linear-response approximation.

In terms of the moments m_k one currently defines [6] average energies E_k by

$$E_k = \sqrt{m_k / m_{k-2}} \tag{2.8}$$

which satisfy the inequalities

$$\cdots \leqslant E_{k-1} \leqslant E_k \leqslant E_{k+1} \leqslant \cdots. \tag{2.9}$$

The mean value $\bar{E}$ and the variance σ of the strength function are trivially given by

$$\bar{E} = \frac{m_1}{m_0}, \tag{2.10}$$

$$\sigma^2 = \frac{m_2}{m_0} - \left(\frac{m_1}{m_0} \right)^2. \tag{2.11}$$

Now, if one wants to fully exploit the RPA sum rule theorems by performing static HF calculations, one can only obtain the moments m_k with odd integer k. Thus the corresponding RPA quantities $\bar{E}$ and σ are not available through static HF calculations alone. The inequalities (2.9) yield, however, the following boundaries for $\bar{E}$ and σ:

$$E_1 \leqslant \bar{E} \leqslant E_3, \tag{2.12}$$

$$\sigma \leqslant \tfrac{1}{2}\sqrt{E_3^2 - E_1^2} = \sigma_{\max}. \tag{2.13}$$

We should emphasize here that in the RPA framework, σ is only representing the so-called escape width (including effects of Landau damping) and does not at all contain the spreading width due to more complicated (e.g., $2p$–$2h$) excitation mechanisms. Therefore, the width evaluated from σ Eq. (2.11) (including a geometrical factor which depends on the form of the resonance curve; for a gaussian its value is $\sqrt{8 \ln 2}$) can be significantly lower than the experimentally observed width. This is particularly so in nuclei and for modes where there is a strong coupling to low-lying shape vibrations.

It is quite clear from the above definitions, that the energies E_k corresponding to different k-values will pertain to different energy domains of collective excitations. For instance, the energy of a slow, adiabatic quadrupole vibration as described in the adiabatic TDHF framework [62] (which is the microscopic version of Bohr's collective Hamiltonian approach [63]) is better represented by E_{-1} than the energies E_1 or E_3. On the other hand, the fast diabatic giant quadrupole resonance is rather accurately described by the energy E_3 (see Section 3.3 below). In more general terms, choosing a given energy E_k not only specifies the operator $\hat{Q}$ which generates it, but also selects an excitation energy regime and the appropriate dynamics or collective path.

For isoscalar local operators $\hat{Q}$ which commute with the potential part of the Hamiltonian $\hat{H}$, the RPA sum rules m_3 and m_1 have a simple physical interpretation [6] in terms of the so-called scaling approach (see Appendix 1.1 for the detailed equations). In this case, the moment m_3^{RPA} turns out to be a stiffness parameter with respect to a scaled HF-energy:

$$m_3^{\mathrm{RPA}} = \frac{1}{2}\left[\frac{d^2}{d\alpha^2} E_{\mathrm{HF}}(\alpha)\right]_{\alpha=0}, \tag{2.14}$$

where

$$E_{\mathrm{HF}}(\alpha) = \langle 0 | e^{\alpha \hat{S}} \hat{H} e^{-\alpha \hat{S}} | 0 \rangle. \tag{2.15}$$

Hereby $|0\rangle$ is the HF ground state and the "scaling operator" $\hat{S}$ is given by

$$\hat{S} = [\hat{T}, \hat{Q}], \tag{2.16}$$

$\hat{T}$ being the kinetic energy operator. The moment m_1^{RPA} is then proportional to the hydrodynamical inertial parameter obtained from a velocity field which is deter-

mined uniquely by the operator $\hat{Q}$ (see Appendix 1.1). It can also be shown [64] to be equal to the Inglis cranking inertia for the collective degree of freedom α.

The energy E_3 can thus be viewed as the one-phonon vibrational energy $\hbar\omega_\alpha$ of the one-dimensional collective Hamiltonian $\hat{H}_{\text{coll}}(\alpha)$ corresponding to the scaling variable α in the harmonic approximation. It should be stressed that in spite of the hydrodynamical nature of the inertial parameter, the stiffness parameter (2.14) includes the effects of the dynamical deformations of the Fermi sphere in momentum space [9, 20] and thus leads beyond purely classical hydrodynamics (see also the discussion in Sect. 2.3 below).

For isovector modes this simple scaling interpretation of the moments m_3^{RPA} and m_1^{RPA} does a priori not apply. The reason is that isovector operators $\hat{Q}$ in general do not commute with the potential part $\hat{V}$ of the Hamiltonian, which leads to considerable complications in the evaluation of the triple commutator in Eq. (2.3b) for m_3. It is then customary to factorize these moments by writing

$$m_1(\hat{Q}) = m_1^0(\hat{Q})(1+\kappa_1), \tag{2.17a}$$

$$m_3(\hat{Q}) = m_3^0(\hat{Q})(1+\kappa_3), \tag{2.17b}$$

where the terms $m_k^0(\hat{Q})$ are evaluated assuming $[\hat{V}, \hat{Q}]$ to vanish, i.e., replacing $[\hat{H}, \hat{Q}]$ by $\hat{S}$ given in Eq. (2.16):

$$m_1^0(\hat{Q}) = \tfrac{1}{2}\langle 0|\,[\hat{Q}, \hat{S}]\,|0\rangle, \tag{2.18a}$$

$$m_3^0(\hat{Q}) = \tfrac{1}{2}\langle 0|\,[\hat{S}, [\hat{S}, \hat{H}]]\,|0\rangle. \tag{2.18b}$$

The coefficients κ_1 and κ_3 are called enhancement factors. For the isovector dipole operator $\hat{D}$ (see also Section 3.2), $m_1^0(\hat{D}) = (\hbar^2/2m)(NZ/A)$ is known as the Thomas–Reiche–Kuhn (TRK) sum rule. The linearity of m_1 with respect to $\hat{H}$ leads to the simple expression

$$\kappa_1 = \frac{1}{2}\,\frac{\langle 0|\,[\hat{Q}, [\hat{V}, \hat{Q}]]\,|0\rangle}{m_1^0(\hat{Q})}, \tag{2.19}$$

whereas κ_3 involves a triple commutator which in general is extremely difficult to evaluate. To the best of our knowledge, only approximate values of κ_3 have been calculated so far for realistic nuclear forces $\hat{V}$ in a generalized scaling approach [65, 66].

We now turn to the discussion of the operator $\hat{Q}$ which in general is not known, except for purely electromagnetic excitation processes. In order to analyze strength distributions and sum rules, one must therefore guess the precise form of $\hat{Q}$. A rather popular form of simple operators with multipolarity L and natural parity $(-1)^L$ is that of Tassie [27]

$$\hat{Q}_L^{(t)} = \sum_{i=1}^{A} r_i^L P_L(\cos\vartheta_i)[1 + I\tau_3(i)] \qquad \text{for} \quad L \geqslant 1, \tag{2.20}$$

and the monopole operator [29]

$$\hat{Q}_0^{(I)} \sum_{i=1}^{A} r_i^2[1 + I\tau_3(i)] \qquad (L=0). \tag{2.21}$$

Hereby $I=0$ gives isoscalar modes and $I=1$ (mainly) isovector modes; τ_3 is twice the third component of the isospin operator. Strictly speaking, $I=1$ leads to pure isovector modes only for symmetric nuclei with $\rho_n = \rho_p$. Otherwise, the operators (2.20), (2.21) with $I=1$ lead to admixtures of isoscalar modes which must be eliminated by specific physical considerations such as, e.g., the conservation of the center of mass in the case of the dipole mode. (See details in Sections 3.1, 3.2 and Appendix 2.)

In particular, for the isoscalar giant quadrupole resonances (2^+, $I=0$), the Tassie operator $\hat{Q}_2^{(0)}$ leads to an excellent agreement (see Section 3.3) of the energies E_3 with the positions of the experimental resonance peaks, the latter practically exhausting the RPA sum rules m_3 and m_1. The situation is similar with the operator $\hat{Q}_0^{(0)}$ for the isoscalar breathing mode (0^+, $I=0$) in heavy nuclei, provided an effective force $\hat{V}$ is used which gives rise to an incompressibility K_∞ of infinite nuclear matter in the range [6] 200 MeV $\lesssim K_\infty \lesssim$ 250 MeV (see Section 3.1). Both isoscalar operators $\hat{Q}_2^{(0)}$ and $\hat{Q}_0^{(0)}$ also give transition densities close to found in RPA calculations [30].

Even for the other known natural-parity modes (with $I=0$ and $I=1$), the Tassie operators give a reasonable guideline for sum rules and peak energy positions. The calculational advantage of these operators is that they lead to simple analytical expressions for m_3, m_1, and κ_1 in terms of the Skyrme force parameters and local densities [6]. For completeness we have compiled all the formulae in Appendix 2. Retaining only the volume terms in a liquid drop model type expansion, one derives easily from these results the typical $A^{-1/3}$-dependence of the energies E_3 for all the isoscalar modes.

From the Tassie operators $\hat{Q}_L^{(0)}$ one automatically obtains the velocity fields of hydrodynamical irrotational flow (see Appendix 1.1). More complicated flow patterns can be obtained in the fluid-dynamical approaches [21, 65–69], where the velocity fields—and thus implicitly the operators $\hat{Q}$—are subject to a variational calculation. From suitable boundary conditions one then obtains a complete set of eigenmodes (with given quantum numbers J^π) which are readily shown [68] to exhaust the m_3 and m_1 sum rules and the lowest of which may directly be compared to the experimental excitation energies. The handicap of this approach is that, in order to keep the calculations tractable, one has to assume liquid-drop like square density profiles and to work with highly schematic forces usually omitting spin-orbit, effective mass, and even Coulomb effects.

In the present work we shall utilize a different approach [70–72]—although similar in spirit—which allows to employ diffuse density profiles and the most sophisticated realistic Skyrme forces (or, in principle, also finite-range forces, see Ref. [73]). The scaling approach is here generalized by introducing several collec-

tive parameters α_i, which are guessed from physical and symmetry considerations, and constructing the corresponding velocity fields. The eigenmodes are then found by diagonalizing the corresponding collective Hamiltonian $\hat{H}_{\text{coll}}(\alpha_i)$. Practically, the number of collective variables α_i is limited. This multidimensional scaling approach is presented in Appendix 1.2. From the formalism presented here, it will become evident that eigenmodes found in this way can be viewed as modes corresponding to one-dimensional scaling vibrations, each with a different operator $\hat{Q}_i$. We shall employ this formalism for monopole and dipole modes in Sects. 3.1 and 3.2 below.

2.2. *Extension to Finite Temperatures*

As suggested by Brink [35], one can consider nuclear giant resonances associated not only with ground states, but also with excited states. Above low (discrete) energies, their theoretical description is rather difficult to perform, except within a statistical approach to equilibrated compound nuclei. As a natural extension of the selfconsistent study of thermodynamical equilibrium properties, one then could perform calculations within the RPA formalism at finite temperature for grand-canonical equilibrium solutions [41]. Alternatively, one can use a finite-temperature sum rule approach to the latter, as sketched below.

Let us assume that the state of the system is defined through a density matrix $\hat{D}$:

$$\hat{D} = \sum_i p_i |i\rangle\langle i|, \tag{2.22}$$

where the sum runs, e.g., over a complete set $\{|i\rangle\}$ of eigenstates of $\hat{H}$ with eigenvalues $\{E_i\}$. As a natural generalization [46, 47, 50, 74] of the strength function one defines

$$S_Q(E) = \sum_{i \neq j} p_i |\langle i| \hat{Q} |j\rangle|^2 \delta[E - (E_j - E_i)] \tag{2.23}$$

and accordingly the moments

$$m_k(\hat{Q}) = \sum_{i \neq j} p_i |\langle i| \hat{Q} |j\rangle|^2 (E_j - E_i)^k. \tag{2.24}$$

It is easily shown [47] that for positive k values the usual sum rule theorems still hold upon defining the relevant expectation values as traces of the product of $\hat{D}$ with the corresponding commutators. For instance, one gets

$$m_1(\hat{Q}) = \tfrac{1}{2}\text{tr}\{\hat{D}[\hat{Q}, [\hat{H}, \hat{Q}]]\}. \tag{2.25}$$

The m_1 sum rule can be shown [47] to be related to the polarisability $\alpha(\hat{Q})$

associated to the Helmholtz free energy of grand-canonical equilibrium solutions ($p_i = Z^{-1} e^{-\beta(E_i - \lambda A)}$, where $\beta = 1/T$ and λ is the chemical potential[2]) by

$$\alpha(\hat{Q}) = 2m_{-1}(\hat{Q}) + \beta\left[\sum_i p_i \langle i|\hat{Q}|i\rangle^2 - \left(\sum_i p_i \langle i|\hat{Q}|i\rangle\right)^2\right]. \tag{2.26}$$

In the above equations, the term proportional to β vanishes whenever $\hat{Q}$ breaks a symmetry of the state $|i\rangle$ or when the set $|i\rangle$ corresponds to a harmonic oscillator spectrum for the variable $Q = \langle \hat{Q} \rangle$. In such cases one retrieves the zero-temperature relation between $\alpha(\hat{Q})$ and $m_{-1}(\hat{Q})$; this holds, of course, in particular in the RPA framework.

Upon replacing the full spectrum of $\hat{H}$ by finite-temperature RPA eigensolutions, one can make use of theorems similar to those proven at zero temperature. For instance the Thouless theorem for m_1 may be generalized [42, 67, 74, 75] as well as similar theorems for m_3 and m_{-1} [50]. These theorems relate (as in the zero-temperature case) hot uncorrelated ground-state properties to sum rules involving correlation effects, or in other words, allow to incorporate the effects of RPA correlations on sum rules while performing only finite-temperature Hartree–Fock (or its semiclassical equivalent) calculations.

Now, to define exactly which density matrix is to be used in a given physical context requires a comparison of two characteristic times: one is a typical time t_c associated with the collective vibration and the corresponding change of the mean field. The other is a relaxation time t_r necessary for the individual particles to adjust themselves to changes of the mean field.

A slow ("adiabatic") collective motion will be characterized by $t_c > t_r$. The density matrices to be used will then typically result from constrained Hartree–Fock calculations (see, e.g., Ref. [76]) yielding both m_{-1} and m_{-3} moments and thus E_{-1} (or E_1) energies. Such processes may a priori be studied in two limiting thermodynamical cases: either in isentropic or in isothermal processes. In the latter case one yields a variation of the entropy S with respect to a "deformation" parameter ε, whereas in the former the temperature T becomes a function of ε.

As an illustrative example for the dependence of T on ε in an isentropic monopole mode, one may develop the following schematic considerations. Let us assume that the nuclear radius in such an adiabatic mode is multiplied by a factor ε. The r.m.s. radius of the selfconsistent mean field will then also be enlarged by the same factor. If this field is roughly approximated by a harmonic oscillator, it is clear that the potential energy (proportional to ω due to the virial theorem) will scale as $\omega^2\varepsilon^2$. Now, the single-particle level density at the Fermi surface, $g(\lambda)$, varies as $1/\omega$, i.e., as ε^2. Let us further assume the degenerate Fermi gas relation between S and T, namely $S = 2aT$, to hold. Since the level density parameter a then equals $\pi^2 g(\lambda)/6$, and due to the isentropic character of the process, one gets

$$T(\varepsilon) = T(1)/\varepsilon^2, \tag{2.27}$$

[2] For the sake of simplicity, we do not distinguish neutrons and protons in this subsection.

where $\varepsilon = 1$ corresponds to the unconstrained thermodynamical equilibrium solution.

In the other limit $t_c < t_r$ one is dealing with a fast ("diabatic") collective motion for which a hot density matrix may be defined by scaling the wavefunctions while keeping the thermal single-particle occupation probabilities unchanged. This clearly corresponds to an isentropic process which is *not* quasi-static and for which no temperature can be explicitly defined. This choice is *inconsistent* with the use of the static entropy density functional (as done in Refs. [48, 50]), since this functional implies the grand-canonical equilibrium variational condition, which is precisely not fulfilled in the diabatic case, and thus leads to a wrong scaling behavior. Quite on the contrary, the entropy should be kept fixed at its static equilibrium value in this case, which is automatically guaranteed when keeping the occupation probabilities unchanged. Clearly, such a dynamical process cannot be described by the moments m_{-3} and m_{-1}, which are explicitly static or adiabatic quantities as discussed above, but is rather well suited for the estimate E_3 of the giant resonance energy through the moments m_1 and m_3. We shall therefore calculate the E_3 energies at finite temperatures accordingly, using the scaling relation Eq. (2.14) (see also the detailed discussion in Appendix 1) with *fixed* occupation probabilities.

2.3. *Density Variational Approach*

We shall now discuss in more detail the way in which the density variational method can be used to calculate sum rules and energies of giant resonances. This method, using Skyrme type effective interactions and ETF (extended Thomas–Fermi) density functionals, has been successfully used [10, 77] as a selfconsistent and, at the same time, very efficient semiclassical substitute for the microscopical HF method in calculating average static properties of nuclei. It becomes particularly gratifying for highly excited nuclei at temperatures $T \gtrsim 2.5$ MeV, where the shell effects vanish [39, 51] and the ETF density functionals become practically exact [52–54]. At zero temperature, the shell effects are explicitly left out in the semiclassical density variational method. Their contributions to the total energy can, however, be recovered perturbatively to a high degree of accuracy [10, 78] by exploiting the Strutinsky energy theorem [39, 79]. Below we shall see to which extent the shell effects in the RPA moments m_k are negligible.

The basic idea of the density variational method is to express the total energy of the nucleus, E, and any other observables (radii, moments m_k, etc.) through the local neutron and proton densities, $\rho_n(\mathbf{r})$ and $\rho_p(\mathbf{r})$, respectively. For the energy one thus writes

$$E = \int \mathscr{E}[\rho_n(\mathbf{r}), \rho_p(\mathbf{r})]\, d^3r. \tag{2.28}$$

The densities ρ_n, ρ_p are found variationally by making the energy (2.28) stationary with the subsidiary conditions

$$\int \rho_n(\mathbf{r})\, d^3r = N, \qquad \int \rho_p(\mathbf{r})\, d^3r = Z. \tag{2.29}$$

At finite temperature T, it is the free energy

$$F = E - TS \tag{2.30}$$

which has to be stationary. In the HF approximation, S is the entropy of noninteracting particles

$$S = -\sum_{q,\,i} [n_i^q \ln n_i^q + (1 - n_i^q) \ln(1 - n_i^q)]; \qquad (q = n, p), \tag{2.31}$$

n_i^q are the Fermi occupation numbers

$$n_i^q = \left[1 + \exp\left(\frac{\varepsilon_i^q - \lambda_q}{T}\right)\right]^{-1} \tag{2.32}$$

in terms of the HF single-particle energies ε_i^q and the chemical potentials λ_q. Writing

$$S = \int \sigma(\mathbf{r})\, d^3r = \int \sigma[\rho_n(\mathbf{r}), \rho_p(\mathbf{r})]\, d^3r \tag{2.33}$$

and using Eq. (2.28), we obtain F as a functional of the densities ρ_q,

$$F = \int \mathcal{F}[\rho_n(\mathbf{r}), \rho_p(\mathbf{r})]\, d^3r, \tag{2.34}$$

and the variational equations become

$$\delta \int \{\mathcal{F}[\rho_n(\mathbf{r}), \rho_p(\mathbf{r})] - \lambda_n \rho_n(\mathbf{r}) - \lambda_p \rho_p(\mathbf{r})\}\, d^3r = 0 \tag{2.35}$$

with the chemical potentials λ_q as Lagrange multipliers.

According to the theorem of Hohenberg and Kohn [80, 81] and its generalisation to finite temperatures [82], the functional (2.34) exists even for a system of correlated fermions. However, it is in general unknown. In the HF approximation using Skyrme type effective interactions,[3] one obtains readily [56] the total HF energy (2.28) in terms of the densities $\rho_q(\mathbf{r})$, the kinetic energy densities $\tau_q(\mathbf{r})$ and spin-orbit densities $\mathbf{J}_q(\mathbf{r})$ (see Appendix 2.1 for explicit expressions). The problem then is reduced to finding the functionals $\tau[\rho]$, $\mathbf{J}[\rho]$, and $\sigma[\rho]$ (for one kind of particles). At low temperatures this is still a difficult task due to the shell effects. In the ETF model [10, 83] the kinetic energy $\tau(\mathbf{r})$ is developed in terms of $\rho(\mathbf{r})$ and its gradients. Such a gradient expansion can also be obtained systematically [84, 85] from the semiclassical Wigner–Kirkwood expansion [86] of the density matrix in powers of $\hbar$. The ETF gradient expansions of $\tau[\rho]$ and $\mathbf{J}[\rho]$ have been generalized to include contributions from effective masses and spin-orbit interac-

[3] The Coulomb exchange energy is, as usual, included in the Slater approximation.

tion, as they arise in connection with the Skyrme forces, both for zero temperature [84, 85] and—together with $\sigma[\rho]$—for finite temperature [52, 53].

We shall not reproduce here the detailed form of the ETF functionals but refer to the literature [10, 53], where it was also shown that the fourth-order gradient corrections are indispensible if one wants to obtain realistic densities $\rho_q(\mathbf{r})$ and at the same time sufficiently accurate total energies. Due to these fourth-order gradient terms, the variations with respect to ρ_n and ρ_p in (2.35) lead to two coupled, highly nonlinear partial differential equations of fourth order which, in general, are quite impossible to solve. We therefore resort to a restricted variational procedure [10] by parametrising the densities $\rho_q(\mathbf{r})$ and minimising F (2.34) with respect to their parameters. For spherical nuclei, with which the present paper is concerned, the following parametrisation is chosen:

$$\rho_q(r) = \rho_{oq}\left[1 + \exp\left(\frac{r - R_q}{\alpha_q}\right)\right]^{-\gamma_q}, \qquad (q = n, p). \tag{2.36}$$

With the restrictions of Eqs. (2.29), this leaves six independent parameters for the variation. The parametrisation (2.36) was found [10, 53] to lead to an excellent agreement of the resulting densities and total energies with averaged HF results. In particular, it has proved to be a very accurate approximation to the exact numerical solutions of the (fourth-order) Euler equation (2.35) for *semi-infinite* nuclear matter at all temperatures [53]. Some slight improvements of the density profiles (with respect to both HF and experimental results) was found by generalising Eq. (2.36), in particular in very light nuclei where desaturation takes place [87] and the densities no longer have a constant bulk region or in very heavy nuclei where the Coulomb repulsion leads to a suppression of the central part of the proton density [10]. These changes of the densities did not, however, affect the total energies by more than a fraction of a million electron volt and will be neglected here. In Table I we have listed the density parameters of Eq. (2.36) which minimize the total energies for a series of spherical nuclei, together with the proton and neutron r.m.s. radii.

The direct application of this density variational method to dynamic nuclear processes is at first handicapped by the fact that the ETF functionals do not apply, in general, to situations where the density is time dependent, except for the case of slow adiabatic processes. In particular, in the study of giant resonances it has been realized [19] that dynamical deformations of the Fermi sphere in momentum space give important contributions to the restoring forces to some modes (e.g., all isoscalar natural parity modes with multipolarity $L \geqslant 2$). This effect, whih in an infinite system leads to Landau zero-sound excitations, has been incorporated to various degree of sophistication in the so-called fluid-dynamical approach and its variations [19–23, 65–69, 88–90]. It is not included, however, in the static ETF functionals which correspond to a spherical momentum distribution [25].

Nevertheless, the ETF density functionals can be used to calculate giant resonance energies, including zero-sound type effects, by properly exploiting the

TABLE I

Density Parameters According to Eq. (2.36) Which Minimize the Total ETF Energy (without C.M. Correction) for 10 Spherical Nuclei, Evaluated with the SkM* Force at Zero Temperature

	ρ_{op} [fm^{-3}]	ρ_{on} [fm^{-3}]	α_p [fm]	α_n [fm]	γ_p	γ_n	R_p [fm]	R_n [fm]	r_p [fm]	r_n [fm]
^{16}O	0.08155	0.08334	0.5726	0.5698	1.406	1.423	2.8675	2.8584	2.68	2.65
^{40}Ca	0.08196	0.08550	0.5947	0.6037	1.493	1.582	4.0101	4.0069	3.38	3.33
^{48}Ca	0.07325	0.09370	0.5668	0.6428	1.520	1.548	4.1848	4.3261	3.45	3.61
^{56}Ni	0.08066	0.08467	0.5943	0.6065	1.488	1.604	4.5143	4.5114	3.72	3.66
^{58}Ni	0.07896	0.08651	0.5873	0.6132	1.499	1.601	4.5541	4.5817	3.73	3.72
^{90}Zr	0.07305	0.08945	0.5710	0.6338	1.503	1.607	5.2656	5.3690	4.21	4.28
^{112}Sn	0.07186	0.08831	0.5648	0.6315	1.472	1.610	5.6810	5.7876	4.52	4.57
^{132}Sn	0.06348	0.09463	0.5451	0.6688	1.467	1.514	5.9140	6.1443	4.67	4.91
^{140}Ce	0.06710	0.09090	0.5505	0.6474	1.459	1.579	6.0940	6.2661	4.81	4.94
^{208}Pb	0.06221	0.09110	0.5315	0.6564	1.401	1.548	6.9670	7.1881	5.47	5.62

Note. r_p and r_n are the proton and neutron r.m.s. radii, respectively.

RPA sume rules m_3 and m_1. Since this a crucial point of our approach, we shall illustrate it here with the example of the isoscalar quadrupole (2^+) giant resonance.

As for all isoscalar modes with a local one-body excitation operator $\hat{Q}$, the m_3 RPA sum rule represents a restoring force parameter with respect to the scaling variable α. Hereby $E_{\mathrm{HF}}(\alpha)$ is the scaled HF energy (2.15). For the Tassie quadrupole operator $\hat{Q}_2^{(0)}$ defined through Eq. (2.20), the main contribution to m_3^{RPA} will come from the single-particle kinetic energy in $E_{\mathrm{HF}}(\alpha)$ (see Section 3.3),

$$m_3^{\mathrm{kin}} = \frac{1}{2}\left[\frac{d^2}{d\alpha^2} E_{\mathrm{kin}}(\alpha)\right]_{\alpha=0} = \frac{1}{2}\sum_q \left[\frac{d^2}{d\alpha^2}\int \tau_q(\mathbf{r}, \alpha)\right]_{\alpha=0} d^3r, \tag{2.37}$$

where $q = n, p$ is the isospin index denoting neutrons and protons, respectively. The kinetic energy density $\tau_q(\mathbf{r}, \alpha)$ is hereby expressed in terms of scaled HF single-particle wavefunctions $\varphi_i^q(\mathbf{r}, \alpha)$ (see also Appendix 2.1) by

$$\tau_q(\mathbf{r}, \alpha) = \frac{\hbar^2}{2m}\sum_{i,q} |\nabla\varphi_i^q(\mathbf{r}, \alpha)|^2. \tag{2.38}$$

In the quadrupole case, the $\varphi_i^q(\mathbf{r}, \alpha)$ are given by [6, 26]

$$\varphi_i^q(\mathbf{r}, \alpha) = e^{-\alpha\hat{S}}\varphi_i^q(\mathbf{r}) = \varphi_i^q(e^{-\eta}x, e^{-\eta}y, e^{2\eta}z) \tag{2.39}$$

with $\eta = (\hbar^2/m)\alpha$. For a spherical nucleus one finds thus easily

$$E_{\mathrm{kin}}(\alpha) = E_{\mathrm{kin}}(\eta) = (2e^{2\eta} + e^{-4\eta})\,\tfrac{1}{3}E_{\mathrm{kin}}(0), \tag{2.40}$$

where $E_{\text{kin}}(0)$ is the kinetic energy in the HF ground state, and thus

$$m_3^{\text{kin}} = 4\left(\frac{\hbar^2}{m}\right)^2 E_{\text{kin}}(0). \tag{2.41}$$

The same relation, replacing $E_{\text{kin}}(0)$ by its classical (or TF) approximation, is also obtained in the fluid-dynamical approach [19, 20] as a consequence of the dynamical deformation of the Fermi sphere in momentum space. This demonstrates that the existence of zero-sound type modes is intimately related to the quantal behaviour of the single-particle kinetic energy in coordinate space [25, 26].

The normal hydrodynamical approach would correspond to replacing $\tau_q(\mathbf{r}, \alpha)$ in Eq. (2.37) by its classical (TF) form proportional to $\rho_q^{5/3}(\mathbf{r}, \alpha)$ with

$$\rho_q(\mathbf{r}, \alpha) = e^{\alpha \hat{S}} \rho_q(\mathbf{r}) = \rho_q(e^{-\eta} x, e^{-\eta} y, e^{2\eta} z). \tag{2.42}$$

This would lead to $m_3^{\text{kin}} = 0$, since the scaling transformation (2.42) is norm conserving and thus the integral over any power of $\rho_q(\mathbf{r}, \alpha)$ is independent of α. Consequently, the ETF functional $\tau[\rho]$ does not have the correct scaling behaviour in the quadrupole case and cannot be used in Eq. (2.37). However, it *first* the derivative $d^2/d\alpha^2$ in Eq. (2.37) is performed on the quantum-mechanical level, leading to Eq. (2.41), and *afterwards* $E_{\text{kin}}(0)$ is replaced by its semiclassical value, obtained with $\tau_{\text{ETF}}[\rho]$, one obtains the correct m_3^{kin} (up to shell effects which are shown below to be negligible).

The operational prescription of our semiclassical approach to the sum rules is thus the following. For a given excitation operator $\hat{Q}$, we first evaluate $E_{\text{HF}}(\alpha)$ and its second derivative in Eq. (2.14) quantum-mechanically and then apply the ETF functionals in evaluating the resulting expression for m_3. The sum rule m_1 is treated accordingly (see Appendix 2). For isovector modes where the scaling concept does not apply exactly or if $E_{\text{HF}}(\alpha)$ is not found easily, one has to go back to the original form of the sum rules given in Eqs. (2.3). The prescription then is analogous. First evaluate the commutators in Eqs. (2.3) quantum-mechanically, then use the ETF density functionals to calculate their static ground state expectation values. In this way, the Landau zero-sound type effects will automatically be built into the results.

It should be noted that the zero-sound effects appear to be negligible in the case of the natural parity monopole (0^+) and dipole (1^-) vibrations. For these modes, the hydrodynamical approach is thus applicable and shall be used in Sections 3.1 and 3.2 below. (See, in particular, a comparison of the two approaches in Table IV and the discussion at the end of Section 3.1.1.)

That the shell effects in the RPA sum rules m_3 and m_1 are small and thus their semiclassical values sufficient for practical purposes, is demonstrated in Fig. 1. Here we have calculated the energy $E_3 = \sqrt{m_3/m_1}$ for three different giant resonances, once microscopically with HF wave functions (crosses) and once using the semiclassical density functional approach (solid lines). The operators chosen for this schematic investigation were the corresponding Tassie operators (2.20), (2.21). The differences to Fig. 1 in Ref. [72] are due to a better parametrisation of the equi-

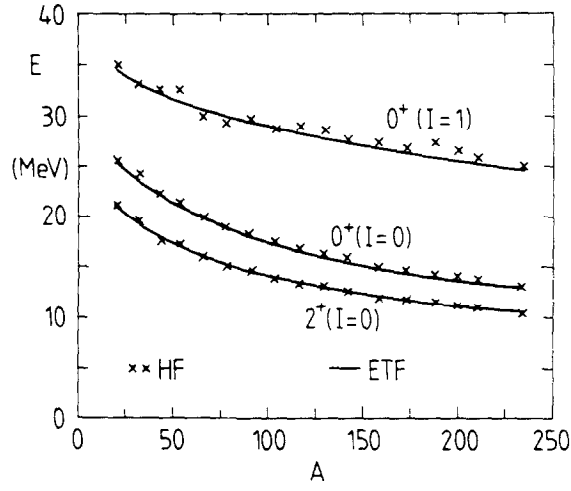

FIG. 1. Giant resonance energies E_3. Solid line: ETF results for nuclei belonging to a smooth fit to the line of β-stability. Crosses: HF results for even–even nuclei close to the β-stability valley. SkM* force used. (See text for the choice of excitation operators.)

librium densities: whereas in Refs. [71, 72] $\gamma_q = 1$ was used in Eq. (2.36), we here take the γ_q which minimize the total ETF energies (see Table I). The enhancement factors in the isovector case (see Section 3.1. for details) were left out for simplicity. The differences between the semiclassical and the microscopical results, due essentially to the shell effects, are seen to be very small. Considering the fact that the uncertainties in the experimental peak energies of the giant resonances are usually of the same order and their widths of the order of 2–4 MeV or more, the semiclassical approximation to the E_3 is thus seen to be excellent.

The situation is less simple for the negative energy-weighted sum rules m_{-1} and m_{-3}, where the shell effects can play a much more pronounced role. In these cases, the semiclassical treatment leads to averaged results only, and microscopical calculations are necessary to obtain quantitative results. Examples thereof will be encountered in Section 3.3 below.

3. Numerical Results

3.1. *Giant Monopole Resonances*

3.1.1. *Isoscalar Monopole Modes*

The isoscalar monopole ($I=0$, $J^\pi = 0^+$) or "breathing mode" has in the last years been used extensively as a tool to study the compressibility of nuclei or nuclear matter. In the classical hydrodynamical model [29] its energy is given by

$$\hbar\omega(0^+) = \sqrt{\hbar^2 K_\infty / m\langle r^2\rangle}, \tag{3.1}$$

where K_∞ is the incompressibility coefficient of infinite nuclear matter, defined by

$$K_\infty = 9\rho_\infty^2 \left.\frac{d^2(E/A)}{d\rho^2}\right|_{\rho=\rho_\infty}. \tag{3.2}$$

Equation (3.1) does, however, not take the finiteness of the nucleus into account; surface, Coulomb, and asymmetry effects are known to reduce the incompressibility of a finite nucleus [30, 91]. It has therefore become customary to define an incompressibility K_A of a *finite* nucleus via its breathing mode (GMR = giant monopole resonance) energy by

$$E_{\mathrm{GMR}} = \sqrt{\hbar^2 K_A / m\langle r^2\rangle}. \tag{3.3}$$

The quantities K_A and $\langle r^2\rangle$ are, of course, model dependent.

In the RPA sum rule approach, one is led to similar expressions, depending on which of the energies E_k, Eq. (2.8) and which excitation operator $\hat{Q}$ one is using. For the isoscalar monopole operator $\hat{Q}_0^{(0)}$, Eq. (2.21), the breathing mode energy E_{GMR} may be identified with E_3 which defines the "scaling incompressibility" K_A^{scal} given in Eq. (A.46) of Appendix 2.2 for a Skyrme force. Identification with E_1 leads to a "constrained incompressibility" K_A^{CHF}. Although these two incompressibilities are different in the limit $A \to \infty$ by a factor $\frac{7}{10}$, they turn out to be rather similar in heavy nuclei (see Refs. [24, 91] for a detailed discussion). This is consistent with the existence of one relatively narrow state containing essentially all of the collective 0^+ strength, as it is found in consistent HF + RPA calculations with effective nuclear interactions [6, 30, 60]. In fact, the RPA energies E_3 fit well the experimental energies of the GMR mode, provided the nuclear matter incompressibility of the force used lies in the range $200\ \mathrm{MeV} \lesssim K_\infty \lesssim 250\ \mathrm{MeV}$. Furthermore, it was found that the operator $\hat{Q}_0^{(0)}$ (2.21) reproduces quite well the RPA transition densities for heavy nuclei. Thus, as discussed in Section 2.1, the scaling approach with the r^2 operator defined in (2.21) seems to work well for this mode.

In the following we shall investigate in some more detail the quality of the scaling approach for the GMR, in particular in light nuclei for which increasing experimental data are becoming available. (For an extensive discussion of the experimental situation up to 1983 on the GMR, we refer to the review by Buenerd [92]. A careful measurement of GMR—and giant quadrupole resonances—in a series of *Sn* isotopes was recently reported in Ref. [93].) We shall first discuss the energy E_3 evaluated with the operator (2.21) for a series of spherical nuclei. The expressions for the moments m_3 and m_1 in terms of the ingredients of the Skyrme HF energy are given in Eqs. (A.45), (A.46) of Appendix 2.2.

In Fig. 2 we compare the HF energies E_3 obtained with different Skyrme forces to the experimental GMR energies for spherical nuclei over the whole mass table. As shown in Fig. 1, there are virtually no shell effects in the energies E_3, so that the semiclassical approximation is fully justified for their evaluation and yields roughly the smooth lines connecting the HF results. It is obvious that most of the forces

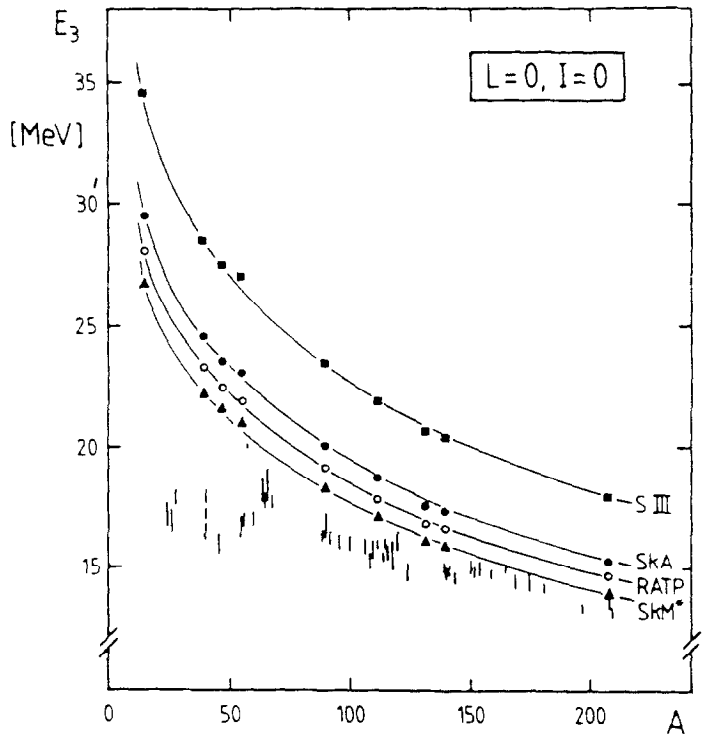

FIG. 2. Breathing mode (GMR) energies E_3, obtained with four different forces (see Table VIII in the Appendix), compared with the experimental energies [92] (represented by the error bars).

give too high energies. Looking at the nuclear matter properties of these forces listed in Table IX, we see that only the forces with $K_\infty < 220$–250 MeV have a chance to yield sufficiently low breathing mode energies, in agreement with the conclusions of Refs. [6, 30]. This is, in particular, the case for the force SkM* obtained [10, 57] by a slight modification of the SkM force which was explicitly adjusted to monopole and quadrupole giant resonances [58]. In fact, with the SkM* force we obtain a good fit of the experimental GMR energies for nuclei with mass number $A \gtrsim 150$. However, for lighter nuclei there is a systematic tendency for the theoretical E_3 energies to overestimate the experimental energies.

According to Eq. (2.12), E_3 is an upper limit for the mean energy $\bar{E}$ (i.e., the centroid of the strength distribution), whereas E_1 is a lower limit. We have therefore also calculated the moment m_{-1} by including a constraint on the squared radius, i.e., by using the monopole operator (2.21) in Eq. (2.4). The derivatives with respect to the Lagrange multiplier λ were done numerically. The uncertainty of this procedure in getting m_{-1} by either of the two expressions on the r.h.s. of Eq. (2.4) was less than 3 %. (See also a somewhat more detailed discussion in Section 3.3.) The results for the different moments are given in Table II for three spherical nuclei, together with the energies E_3 and E_1. We see that the difference between these two

TABLE II

Sum Rules (with r^2 Operator), Energies, and Widths of the Isoscalar Breathing Mode (GMR), Obtained for Three Spherical Nuclei with the SkM* Force

	m_3 [10^7fm^{4}MeV^3]	m_1 [10^4fm^{4}MeV]	m_{-1} [10^2fm^{4}MeV^{-1}]	E_3 [MeV]	E_1 [MeV]	E_{exp} [MeV]	Γ_{max} [MeV]	Γ_{exp} [MeV]
^{40}Ca	1.87	3.73	0.82	22.4	21.3	(16–18)	8.0	
^{90}Zr	4.48	13.5	4.30	18.3	17.7	16.2	5.4	3.5 ± 0.3
^{208}Pb	10.1	53.4	29.5	13.8	13.4	13.8	3.5	2.8 ± 0.5

Note. Experimental values from Ref. [92].

energies is varying by about 1 to $\frac{1}{2}$ MeV from light to heavy nuclei. This cannot account for the systematic discrepancy observed above for the light nuclei, the energy E_1 there still being too high. Table II also contains the upper limits Γ_{max} for the width, evaluated from σ_{max}, given in Eq. (2.13), using the relation $\Gamma_{max} = \sqrt{2 \ln 8}\sigma_{max}$ valid for a gaussian form of the strength distribution.

We shall now address the problem of the GMR energies in light nuclei. RPA calculations indicate [30, 60] that there is a tendency of the giant resonances to be much more fragmented in light nuclei than in the heavy ones. This is, of course, difficult to check in the sum rule approach. Within our semiclassical approach we are, however, able to investigate the question of the choice of the operator $\hat{Q}$ or, classically speaking, the question which is the right collective degree of freedom to describe the breathing mode. In particular, we can study the role of the surface as a dynamical variable, which certainly is becoming more important in lighter nuclei. This question has been addressed within the semiclassical density variational framework in Refs. [70, 71]. There the scaling model was extended to two coupled modes, taken to be a surface and a bulk density vibration. Starting from the parametrization (2.36) of the proton and neutron densities, one may consider the surface diffusivities α_q and the central densities ρ_{oq} as independent collective degrees of freedom (the radii R_q being adjusted at any time to conserve the particle numbers Z, N, and the γ_q being kept constant). For an isoscalar mode, one has to let the proton and the neutron parameters be in phase, for an isovector mode they have to be in opposite phase (see Section 3.1.2 below). For one particular coupling between the α_q and the ρ_{oq} (see the discussion below) one obtains the usual one-dimensional scaling vibrations corresponding to evaluating the RPA energy E_3 with the monopole operator (2.21). Treating them as independent degrees of freedom, one obtains two coupled modes which can be diagonalized (as described in detail in the Appendix 1.2 on the multidimensional scaling model). This procedure has been followed for the isoscalar GMR in Refs. [70, 71] and for the isovector GMR in Refs. [70, 72]. In Ref. [70], the Skyrme force SIII was used which leads to too high breathing mode energies due to the large value of K_∞ of this force. In Refs. [71, 72] the force SkM* was used; we present here an improvement of these results.

Figure 3 shows the results obtained with the force SkM*. Crosses indicate again

the HF energies E_3 obtained with the monopole operator (2.21), thus corresponding to the usual one-dimensional scaling. The open squares indicate the positions of the lower of the two eigenmodes found from the semiclassical 2-dimensional scaling described above. For $A \gtrsim 100$, the two practically agree and fall on the LDM curve proportional to $A^{-1/3}$ indicated by the solid line. However, for lighter nuclei the results from the 2-dimensional scaling calculation lie much lower in energy, coming in fact close to the experimental ones. (In Refs. [71, 72] this effect was found to be smaller due to the neglect of the degrees of freedom γ_q in the density parametrisation (2.36), i.e., to fixing $\gamma_q = 1$. In the present work, the variational values of γ_q—see Table 1—have been used.) We see that the role of the surface diffusivities α_q as independent collective degrees of freedom becomes very important for a correct description of the breathing mode in light nuclei. This is not very surprising since the properties of these nuclei are mostly dominated by their surface.

In Table III we present the energies of the diagonalized eigenmodes for spherical nuclei, both for isoscalar and isovector monopole vibrations (see Section 3.1.2 for the discussion of the latter). The lower energy for each nucleus corresponds to the squares in Fig. 3.

Also shown in Table III are the percentages of the energy-weighted (m_1) sum rule for the monopole operator (2.21). We see that for the light nuclei a lot of r^2 strength is missing in the lower mode (up to about 60 %), which is in good agreement with experimental findings [92]. This strength lies in the upper mode which is presumably very difficult to observe experimentally due to its high energy.

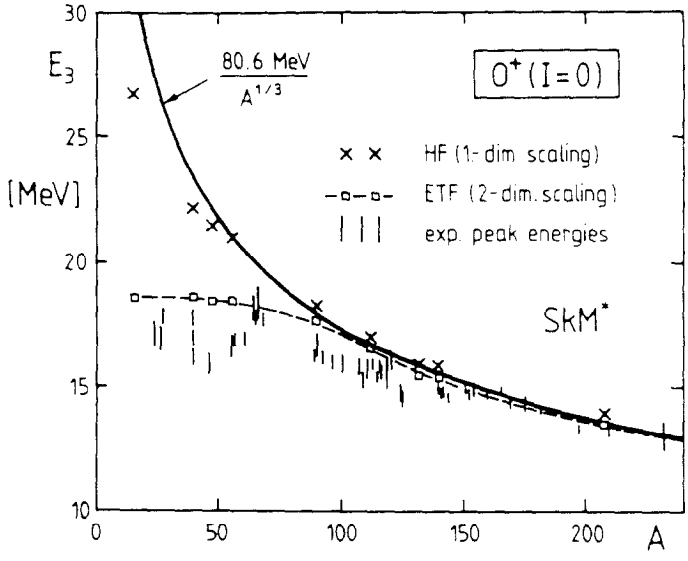

FIG. 3. Breathing mode (GMR) energies obtained with the SkM* force. Crosses: HF energies E_3 with operator (2.21), as in Fig. 2. Squares: lowest of two coupled modes from 2-dimensional scaling of ETF densities. Error bars: experimental values as in Fig. 2. Solid line: LDM fit proportional to $A^{-1/3}$.

TABLE III

Breathing Mode (GMR) Energies Obtained in the Generalized 2-Dimensional Scaling Approach by Coupling Bulk Density and Surface Vibrations of Both Isoscalar ($I=0$) and Isovector ($I=1$) Type

	$I=0$					$I=1$				
	$\hbar\omega_i$ [MeV]	β_i	$\bar{E}_{exp}$ [MeV]	$\%(m_1)$	$\%(m_3)$	$\hbar\omega_i$ [MeV]	β_i	$\bar{E}_{exp}$ [MeV]	$\%(m_1)$	$\%(m_3)$
^{16}O	29.9	+0.25		50.5	72.4	39.6	+0.15		68.9	88.7
	18.6	+3.5		49.5	27.6	21.0	+1.7		31.1	11.3
^{40}Ca	24.0	+0.45	(16–18)	55.5	67.4	35.2	+0.23	31.1 ± 2.2	79.3	90.6
	18.6	+9.5		44.5	32.6	22.2	+2.7		20.7	9.4
^{48}Ca	23.4	+0.64		41.6	53.3	34.4	+0.30		78.0	88.8
	18.5	−24		58.4	46.7	23.0	+3.2		22.0	11.2
^{58}Ni	22.5	+0.84	17.1 ± 0.3	32.6	40.7	33.9	+0.36	30.6 ± 2.3	78.1	87.9
	18.9	−5.1		67.4	59.3	23.7	+3.8		21.9	12.1
^{90}Zr	22.8	+1.8	16.2 ± 0.5	2.6	4.2	32.3	+0.79	28.5 ± 2.6	62.9	72.4
	17.7	−0.84		97.4	95.8	26.0	+9.9		37.1	27.6
^{112}Sn	23.2	+2.4	15.88 ± 0.14	0.3	0.6	31.8	+1.7		48.0	56.7
	16.7	−0.51		99.7	99.4	26.7	−102		52.0	43.3
^{132}Sn	23.2	+2.5		0.4	1.0	31.7	+1.6		27.8	35.5
	15.5	−0.57		99.6	99.0	26.5	−5.8		72.2	64.5
^{140}Ce	24.3	+2.9	14.8 ± 0.2	0.0	0.1	32.5	+1.9	27.5 ± 2.6	19.0	25.2
	15.6	−0.39		100.0	99.9	27.1	−3.7		81.0	74.8
^{208}Pb	23.7	+3.8	13.8 ± 0.5	0.1	0.2	32.0	+3.1	26.0 ± 3.0	5.6	8.3
	13.5	−0.23		99.9	99.8	26.0	−1.7		94.4	91.7

Note. Second column: the two eigenfrequencies $\hbar\omega_i$; third column: coupling parameters β_i defined in Eq. (3.4); fourth column: experimental GMR energies [92, 93, 95]; fifth and sixth columns: percentages of the m_1 and m_3 sum rules, evaluated for the operators (A.43) for $I=0$ and (A.47) for $I=1$. (See Subsection 3.1.2 for the discussion of the isovector results.)

As discussed in Ref. [71], the coupling of the parameters α_q and ρ_{oq} may be described in terms of a coupling parameter β by

$$\frac{\alpha_q(t)}{\alpha_q(0)} = \left[\frac{\rho_{oq}(t)}{\rho_{oq}(0)}\right]^{\beta}. \tag{3.4}$$

The usual one-dimensional scaling (i.e., calculating the energy E_3 with the r^2 excitation operator) corresponds to $\beta = -\frac{1}{3}$, while a pure bulk-density vibration with fixed α_q is given by $\beta = 0$. Larger absolute values of β mean a stronger participation of the surface diffusivity in the vibration.

Due to Rayleigh's variational principle [94], the two diagonalized eigenmodes may be visualized as one-dimensional vibrations with fixed β, its value being found

by minimizing and maximizing, respectively, the energy of this one-dimensional mode [71]. In principle, one can obtain the operators corresponding to the diagonalized modes by integration of the orthogonal velocity fields, but this can only be done numerically. The values of β found for the two coupled modes are also given in Table III. We see that the lower modes in the heavy nuclei are not much different from the usual one-dimensional scaling ($\beta \simeq -\frac{1}{3}$), whereas in the lighter nuclei their values of β becomes larger in magnitude, implying a stronger surface component of the vibration.

In a series of S_n isotopes the isoscalar GMR and giant quadrupole (GQR) centroid energies have recently been determined experimentally [93] with a rather high accuracy. In Fig. 4 we show these data together with our theoretical results, assuming these nuclei all to be spherical. In the upper part of the figure the GMR energies are seen. The upper line corresponds to the one-dimensional scaling case (i.e., energy E_3 with the r^2 operator); the lower line represents the lowest of the two coupled modes, obtained as discussed above. As for all nuclei in this region, our results overestimate the experimental GMR energies by about 0.6–0.8 MeV. The isotopic A-dependence, however, is in excellent agreement with experiment.

The experimental GMR energies of Ref. [93] have recently been used [96] to determine the leading coefficients of a phenomenological LDM type expansion of the compressibility K_A in Eq. (3.3), using experimental values of $\langle r^2 \rangle$. This analysis favours values of the volume term K_v of ~ 300 MeV. We refer to Section 4 for a discussion of this point.

With the formalism presented in Appendix 1.2 it is easy to calculate the transition

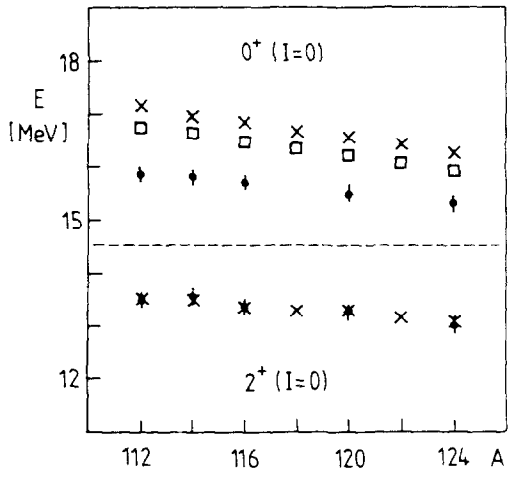

FIG. 4. Upper part of figure: Breathing mode (GMR) energies of Sn isotopes. Crosses: 1-dimensional scaling (i.e., energies E_3 with operator (A.43)). Squares: lowest of two coupled modes, as in Fig. 3 and Table III. Dots with error bars: experimental data from Ref. [93]. Lower part of figure: Giant quadrupole resonance (GQR) energies for the same nuclei. (See Section 3.3 for the discussion.) Crosses: Energies E_3 with quadrupole operator (A.59). Dots with error bars: experimental data from Ref. [93]. SkM* force used.

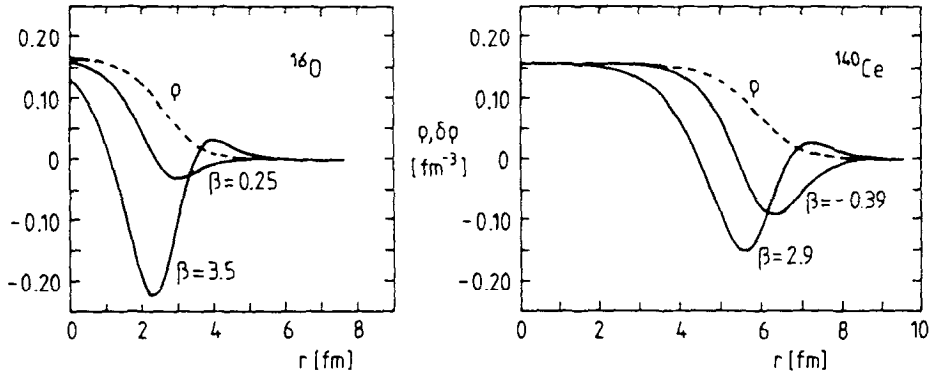

FIG. 5. Transition densities obtained with the SkM* force for the GMR modes of the nuclei ^{16}O and ^{140}Ce. The values of β (see text for the discussion), as found in Table III, are shown along the corresponding curves. The dashed lines show the ground-state densities ρ of these nuclei.

densities—see Eq. (A.31)—of the the eigenmodes for a given nucleus. As an example, we show in Fig. 5 the transition densities for the two eigenmodes of the isoscalar GMR in ^{16}O and ^{140}Ce. The value of the coupling parameter β, seen in Table III, are shown along the corresponding curves. (The dashed lines show the ground-state densities $\rho(r)$ of these nuclei.) The transition density of the lower mode in ^{140}Ce, having one node in the surface region, is typical for the GMR in heavy nuclei and is obtained both semiclassically here (see also the corresponding curve for ^{208}Pb in Ref. [71]) and microscopically in RPA calculations [30, 60]. The transition densities found in our present semiclassical approach for the upper modes (dominated by the surface vibrations) in heavy nuclei, typically have two nodes in the surface region. Note that a high-lying collective isoscalar 0^+ state with a similar transition density has also been found in microscopical HF-RPA calculations [97]. In the light nuclei, for which we show the example of ^{16}O in Fig. 5, the situation is reversed: the transition densities of the lower (upper) modes have two nodes (one node) in the surface. It would be interesting to compare this prediction with an analysis of experimental data in light nuclei.

We finally want to address briefly the technical question, raised in Section 2.3, of evaluating the restoring force parameters before or after introducing the semiclassical ETF density functional for the kinetic energy. As discussed there, taking the second derivative with respect to α in Eq. (2.37) *before* making the semiclassical approximation is essential in the case of the giant quadrupole resonance, in order not to miss the effects which are linked to a dynamical deformation of the Fermi sphere in momentum space and which—at least for that case—bring about a big difference to the hydrodynamical approach corresponding to a scaling of the semiclassical (ETF) energy. However, in the above calculations of the coupled monopole surface and bulk density vibrations, we have evaluated the restoring force matrices (corresponding to the generalized scaling energies E_3) after use of the ETF kinetic energy density functional, since these two collective degrees of freedom

can only be defined in a semiclassical way and a quantum-mechanical evaluation of the corresponding restoring forces is not possible. In the one-dimensional scaling case, the quantum-mechanical evaluation of E_3 is simple (see Appendix 2.2) and it is possible to check explicitly the difference of the two approaches. In fact, it is easy to see that the only difference comes about through the effective mass terms in the kinetic energy density functional (see Ref. [10] for these terms). In Table IV we show the errors in the energies E_3 coming from these terms when scaling numerically the ETF kinetic energies. They are seen to be of the order of 1–3 % only and thus smaller than the uncertainties in both theory (e.g., due to the choice of the interaction) and experiment. This seems to justify our approach used here for the giant monopole vibrations, which is essentially hydrodynamic in nature.

To summarize the results of this section, we may conclude that a reasonable understanding of the isoscalar GMR is obtained in terms of a semiclassical, hydrodynamical picture which is a straightforward extension of the usual scaling model corresponding to the HF-RPA calculation of the energy E_3.

We should stress that we have not discussed here the effects of nuclear deformation. A static deformation of the ground state will couple the monopole and β-type quadrupole 0^+ modes (see, e.g., Ref. [64]). In light nuclei or in soft transition nuclei, the effects of this coupling may become important. In this connection it will also be interesting to study in detail the isoscalar giant monopole and quadrupole resonances recently measured in a series of *Sm* isotopes [93]. It is straightforward to apply the extended scaling model for coupled modes, presented here, to deformed nuclei. Work in this direction is in progress; preliminary results seem to indicate [98] that the effect of a static deformation on the uncoupled GMR is inferior to 1 MeV, in agreement with the results of the schematic estimates of Ref. [64].

3.1.2. *Isovector Monopole Modes*

It will only take little space to discuss the case of the isovector ($I=1$) giant monopole resonances which recently have been studied carefully in pion-induced charge exchange reactions (see the review by Bowman [95]). In our calculations, we have used the same semiclassical scaling approach as discussed above, coupling surface diffuseness and bulk density vibrations, except now the vibrations of ρ_{vq} and α_q for protons and neutrons are taken to be opposite in phase.

TABLE IV

Energy E_3 (as in Table II) and Error ΔE_3 Due to Numerical Scaling of the ETF Kinetic Energy Functional

Nucleus	^{16}O	^{40}Ca	^{48}Ca	^{56}Ni	^{90}Zr	^{112}Sn	^{132}Sn	^{140}Ce	^{208}Pb
E_3 [MeV]	26.02	22.41	21.26	20.68	18.26	17.11	15.83	15.85	13.78
ΔE_3 [MeV]	0.82	0.49	0.55	0.39	0.29	0.25	0.23	0.22	0.16
% error	3.2	2.2	2.6	1.9	1.6	1.5	1.4	1.4	1.2

Quantum-mechanically, the isovector giant resonances have one unit of isospin I compared to the ground state and, thus, three components of I_3 which can be selectively excited experimentally (see, e.g., Ref. [99] for a discussion). Our semiclassical description can, however, not distinguish these three components. Therefore, the semiclassical energies must be compared to the average positions of the corresponding isospin triplets.

Our results for the eigenmodes and sum rules have been included in Table III above. In contrast to the case of the isoscalar GMR, the isovector r^2 strength is found to be carried by the lower modes only to 80–90 % in heavy nuclei, and even only to 20–30 % in the light nuclei. This is demonstrated graphically in Fig. 6, where for each nucleus the two energies ($\hbar\omega_i$ in Table III) are shown in circles. The black area in each circle corresponds to the percentage of the isovector r^2 sum rule m_1, evaluated with the operator (A.47), carried by that state. The isospin-averaged experimental energies are shown with their error bars by the triangles. They are seen to be closer, on each side of the mass region, to the state that carries most of the strength according to our calculation.

We should mention that our present approach neglects the enhancement factors appearing in the quantum-mechanical evaluation of the m_3 and m_1 RPA sum rules (see Eqs. (2.17)–(2.19) in Section 2); the (generalized) scaling approach only takes into account the contribution of the parts m_k^0 defined in Eq. (2.18). The calculation of κ_3 in (2.17b) is extremely tedious and has, to our knowledge, not been carried out so far. Although the effects of κ_1 and κ_3 might be included approximately in a

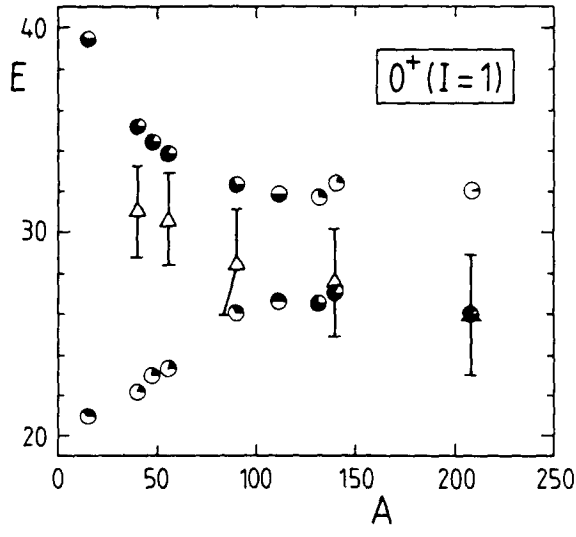

FIG. 6. Isovector GMR energies evaluated in the generalized semiclassical scaling approach with the force SkM*. The circles give the positions of the two eigenmodes ($\hbar\omega_i$ in Table III) obtained by coupling isovector surface diffuseness and bulk density vibrations. The black area inside each circle represents the m_1 strength (see Table III) carried by that state. The experimental points (triangles) show the isospin-averaged energies taken from Ref. [95].

somewhat ad hoc way in the scaling model [66, 107], we preferred to present our results here without this estimate. (For a semiclassical calculation of κ_1, see Ref. [72].) In view of the uncertainties with respect to the omission of the enhancement factors κ_k on one hand, and the experimental error bars on the other, the agreement found in Fig. 6 is quite satisfactory.

3.2. *Isovector Giant Dipole Resonances*

We will restrict our discussion of the electric dipole mode to the isovector case which has been originally interpreted by Goldhaber and Teller [2] as a collective motion of protons and neutrons in opposite phase along a given spatial direction. This collective vibration is mainly observed in photoabsorption reactions. In this case, the excitation operator $\hat{Q}$ is unambiguously given by the electric dipole operator,

$$\hat{D} = \sum_{i=1}^{Z} (z_i - \zeta), \tag{3.5}$$

where the sum runs over the protons and where z_i and ζ are the z-coordinate of the proton labelled i and the center of mass of the whole nucleus. This operator can be easily written in the form of Eq. (A.54) including then an isoscalar and an isovector part.

As a consequence of the knowledge of the excitation operator, the m_k sum rules are related to the experimentally measured photo-absorption cross sections $\sigma(E)$ by the energy-integrated cross sections through

$$\sigma_k = \int \sigma(E) \cdot E^k \cdot dE = 4\pi^2 \frac{e^2}{\hbar c} \cdot m_{k+1}, \tag{3.6}$$

leading thus to a direct experimental test of the m_k moments of the strength distribution. As a first example, the enhancement factor κ_1 (see the general expression of Eq. (2.19) and the expressions (A.56), (A.57) for Skyrme-like forces) can be calculated theoretically and compared to the values extracted from the inegrated experimental cross sections σ_0. Our theoretical m_1 and κ_1 values calculated with the SkM* force are shown in Table V together with the results for m_{-1} and E_1. They are found to be slowly increasing as a function of the mass number A in agreement with the experimental behaviour.[4] Nevertheless, there appears a large discrepancy in the absolute magnitude [31, 47]. This deviation is mainly due to the high-energy component of $\sigma(E)$ included in σ_0 through the integration appearing in Eq. (3.6). At these energies one should take into account π-threshold effects which of course are not included in our evaluation of the κ_1 enhancement factor. Moreover, short-range two-body correlation effects play a very important role there. One should think of treating them in a phenomenological effective way. It is known that the tensor interaction is most relevant for that. However, in the current parametrisation of the Skyrme-like effective interactions, a tensor force is not explicitly included. (It was

[4] We take into account here experimental results which yield low κ_1 values for light nuclei [104].

TABLE V

Sum Rules m_{-1}, m_1, Energy E_1, and Enhancement Factor κ_1 for the GDR Obtained Semiclassically (SC) with the SkM* Force

	m_{-1} [MeV^{-1}fm^2]		m_1 [MeVfm^2]		E_1 [MeV]	E_{exp} [MeV]	κ_1	E_{DM} [MeV]
	SC	Exp	SC	Exp	SC	Exp		
^{16}O	0.215	0.205 ± 0.004	107.0	116 ± 12[a]	22.3	23.8 ± 0.5	0.291	23.5
^{40}Ca	0.682	0.780 ± 0.016	279.6	446 ± 41[b]	20.2	19.8 ± 0.5	0.349	20.8
^{48}Ca	0.861	—	328.4	—	19.5	—	0.358	19.8
^{56}Ni	1.069	—	395.8	—	19.2	—	0.364	19.6
^{90}Zr	2.054	1.63	636.8	808 ± 68	17.6	16.5 ± 0.2	0.382	17.7
^{140}Ce	3.889	3.67 ± 0.26	980.6	1210 ± 110	15.9	15.0 ± 0.1	0.393	15.8
^{208}Pb	7.047	7.35 ± 0.51	1439	1840 ± 150	14.3	13.5 ± 0.2	0.397	14.2

Note. Experimental values are from Ref. [103] except for (a) ^{16}O (data of Ref. [104]) and for (b) ^{40}Ca (older data of Ref. [105]; see Refs. [104, 106] for a discussion concerning this point). The last column contains the estimates of the GDR energy from the improved droplet model (DM) formula of Ref. [31].

argued [56] that its contribution to the ground-state energy has partially been taken into account in the central and spin-orbit terms of the effective force. This "renormalization" of the effective force can, however, not be expected to apply also to the calculation of the RPA moments under discussion here.) The behaviour of κ_1 as a function of A, as well as the discrepancy discussed above, appear also for the Gogny effective interaction [100] which does not include any tensor term, either. Consequently, these shortcomings do not seem to depend on the zero-range or finite-range character of the central part of the force.

As we have seen in Section 2.1, the RPA m_{-1} sum rule must be evaluated through a contrained Hartree–Fock (CHF) calculation. For the ($J^\pi = 1^-$, $I = 1$) mode, such calculations have been performed [101]. In order to avoid such rather time consuming calculations as well as many numerical difficulties appearing in CHF calculations, it is interesting to develop simple approximations mainly based upon the restriction of the variational space used in the constrained HF problem.

The simplest approximation is to assume a pure scaling of the wave functions. Using the operator $\hat{Q} = \hat{D}$ of Eq. (3.5), this corresponds exactly to the Goldhaber–Teller (GT) description of the dipole resonance, where neutrons and protons are displaced opposite to each other without change of their respective densities. In the description of Migdal [4], the two densities are compressed and decompressed, without displacing their surfaces, in such a way that a dipole oscillation is generated. Both these modes have been used in the liquid drop model (LDM) framework [4, 11, 12, 31] for m_{-1} sum rules and energies $E_3^0 = \sqrt{m_3^0/m_1^0}$. The conclusion was that a suitable combination of the Goldhaber–Teller and the Migdal modes is required to correctly describe the systematics of the GDR peak energy positions.

The calculation of m_{-1} for the Migdal mode can naturally be improved using the droplet model [31, 102]. However, the results remain too low compared to the experimental σ_{-2} values. This discrepancy gives us the hint that here, too, one should better consider a coupling between Tassie and Migdal modes. For that purpose, we use the semiclassical ETF density functional method to solve the constrained variational problem $\delta\{\langle \hat{H} - \lambda \hat{D} \rangle\} = 0$ with the following trial functions for the polarized densities ρ_q ($q = n, p$ respectively):

$$\rho_q = \rho_q^0 + \varepsilon_q z \rho_q^0 + \eta_q (\partial \rho_q^0 / \partial z). \tag{3.7}$$

Here ρ_q^0 denotes the equilibrium density whereas ε_q and η_q are variational deformation parameters. The m_{-1} moments have then been calculated as polarisabilities according to Eq. (2.4). As compared to a simple GT or Migdal mode, one gets [41, 109] significantly increased m_{-1} values. Such results, included in the first column SC of Table V, agree fairly well with the experimental values extracted from integrated cross sections σ_{-2}. From our results for m_{-1} and m_1, one may evaluate E_1 energies whose trend obviously reflects the deficiency of our estimate for m_1 discussed above (too low by $\sim 20\%$). Also shown in Table V is the energy E_{DM} obtained from the droplet model formulae [31] for m_{-1} and m_1 corresponding to the Migdal mode (improved as described above). The good overall agreement of E_{DM} with the experimental GDR peak energies is, however, rather accidental since both moments separately are too small as already mentioned.

We finally discuss the calculation of E_3 energies in the generalized scaling approach. As in the isovector monopole case (see Section 3.1), we have calculated E_3^0 (i.e., neglecting the enhancement factors κ_k) for the dipole operator (3.5) corresponding to the pure Tassie mode. Table VI gives in the first column the results E_{Tassie} so obtained with the SkM* force for some spherical nuclei. Not only are the values systematically too low for all considered nuclei, but the trend of their A-dependence is wrong (the relative discrepancy with $\bar{E}_{\mathrm{exp}}$ constantly decreases from 18% in ^{16}O to 4% in ^{208}Pb).

We have therefore extended the scaling approach by a diagonalization of two coupled modes according to the method of Appendix 1.2 which we have successfully used for the GMR resonances (see Section 3.1). We have hereby coupled the Tassie mode with the Migdal mode defined through the variables η_q in the last term of Eq. (3.7). The scaling energies E_3 corresponding to this pure Migdal mode are given in the second column in Table VI. The two eigenmodes E_i obtained after diagonalisation of the two-dimensional problem are given in the third column. The contributions (in percent) of these eigenmodes to the dipole m_1 sum rule are also given. The lowest eigenenergies are to be compared with the observed energies of the resonance. Again and as expected, the calculated values are found even lower than in the uncoupled case with respect to experimental values. However, the bulk variation is correct since the relative discrepancy lies systematically in the vicinity of 16%.

One ought to assess now the effect of the neglected enhancement factors κ_1 and κ_3. The mean energies m_1/m_0, calculated with the eigensolutions in Table VI, are

TABLE VI

Energies (in MeV) of the Isovector Electric Dipole Giant Resonance for Various Collective Modes

Nucleus	E_{Tassie}	E_{Migdal}	E_i	% m_1	$\bar{E}^{\text{av}}_{\text{exp}}$	$\bar{E}_{\text{exp}}$
^{16}O	19.8	20.9	40.9 19.8	0.0 100.0	25.4	23.8 ± 0.5
^{40}Ca	17.5	18.0	30.9 17.2	1.3 98.7	20.3	19.8 ± 0.5
^{48}Ca	17.0	17.3	29.4 16.6	1.9 98.1	19.4	19.5 ± 0.5[a]
^{56}Ni	16.7	16.9	28.8 16.3	2.6 97.4	18.7	—
^{90}Zr	15.4	14.9	25.9 14.5	5.8 94.2	16.7	16.5 ± 0.2
^{140}Ce	14.1	13.0	23.4 12.7	9.5 90.5	15.0	15.0 ± 0.1
^{208}Pb	13.0	11.4	21.5 11.3	12.5 87.5	13.7	13.5 ± 0.1

Note. The SkM* force is used here. $\bar{E}_{\text{exp}}$ are experimental energies [103] while $\bar{E}^{\text{av}}_{\text{exp}}$ are smoothed energies obtained from the empirical formula [5] $\alpha A^{-1/6} + \beta A^{-1/3}$. For ^{48}Ca, the value (a) concerns the lowest isospin component of the GDR [108].

found to be ~ 2.5 MeV lower than the E_1 energies of Table V which have been evaluated including the enhancement factor κ_1. Due to the inequality (2.12) which is thus violated, we can anticipate that the correct inclusion of κ_1 and κ_3 will shift the spectrum upwards by at least 2.5 MeV. A crude estimate of the "enhanced" uncoupled E_3 energies consists [107] in multiplying the corresponding E_3^0 values by a factor of $\sqrt{1+\kappa_1}$. When doing so with the values of κ_1 listed in Table V, one obtains indeed the experimental values within ~ 1 MeV.

In summary, the GDR is thus found to have a small Migdal component, from 0 % in ^{16}O (where the surface mode is of course dominant) to ~ 10–12 % in heavy nuclei, where it lowers the energies by about 1–2 MeV. This trend is similar to that observed in the results for the m_{-1} sum rule using the same two-dimensional variational space.

3.3. *Giant Quadrupole Resonances*

In this section we evaluate sum rules and energies associated with the axial quadrupole operator[5]

$$\hat{Q} = r^2 P_2(\cos\theta) = \tfrac{1}{2}(2z^2 - x^2 - y^2) \tag{3.8}$$

[5] For consistency with the general definition (2.20) of the Tassie operators, we take here half the usual spectroscopic quadrupole operator (see, e.g., Ref. [11]).

which creates isoscalar quadrupole vibrations ($I=0$, $J^\pi=2^+$). Similarly to the case of other isoscalar modes, the moments m_1 and m_3 have been calculated semiclassically (see Section 2.3 and Appendix 2.5).

For this mode, we have also performed calculations of the moments m_{-1} and m_{-3} which do not belong to a density variational approach but are done on a strictly microscopical level, in order to demonstrate the necessity for such calculations of quantities which are strongly affected by shell structure. Due to the availability of the numerical methods detailed in Refs. [34, 76] we have evaluated these moments within the adiabatic TDHF framework, which amounts to a CHF calculation with the external field $\hat{Q}$ yielding m_{-1}, and another CHF calculation with the external field $\hat{P}$ defined in Eq. (2.6) yielding $m_{-3}/(m_{-1})^2$.

Let us discuss briefly some calculational details in order to assess the numerical accuracy of the calculated values for m_{-1}, m_{-3} and thus E_{-1}. HF single-particle states have been expanded on 13 harmonic oscillator shells for ^{208}Pb and 11 shells for all other nuclei. Increasing the basis from 11 to 13 shells in ^{208}Pb yields an increase of m_{-1} by about 6 % and a decrease of m_{-3} by about 11 %. This results in an increase of E_{-1} by some 8.5 % which therefore represent a reasonable upper bound of the numerical error associated with the basis truncation. To evaluate the m_{-1} moments, we have performed CHF calculations around the equilibrium quadrupole moment Q_0 (which is zero in all nuclei here). The polarisability may then be deduced in various ways as sketched above in Section 2.1. The spread of the numerical results obtained by the different methods never exceeds 3 % of the average values retained here.

Table VII displays our results obtained with the SkM* force for some spherical nuclei. Selfconsistent corrective terms similar to those introduced by Thouless and Valatin for the rotational mode [110] have been included. Their omission, which would correspond to the Inglis cranking approximation [111], would lead to an underestimation of m_{-1} by about 5 % for all nuclei considered here.

In order to compare the various moments calculated for different nuclei, it is useful to discuss the global A-dependence which is of the form $A^{2-k/3}$ for the

TABLE VII

Sum Rules and Energies for the GQR Obtained with the SkM* Force for Some Spherical Nuclei

	m_{-3} [fm^{4}MeV^{-3}]	m_{-1} [10^{2}fm^{4}MeV^{-1}]	m_1 [10^{3}fm^{4}MeV]	m_3 [10^{7}fm^{4}MeV^3]	E_{-1} [MeV]	E_1 [MeV]	E_3 [MeV]	σ_{max} [MeV]
^{16}O	0.029	0.114	4.77	0.208	20.0	20.5	20.9	2.0
^{40}Ca	0.225	0.660	19.2	0.568	17.1	17.1	17.2	1.1
^{48}Ca	20.4	2.75	24.9	0.736	3.67	9.53	17.2	7.2
^{56}Ni	73.5	6.75	31.1	0.893	3.03	6.79	16.9	7.8
^{90}Zr	135	18.1	67.6	1.39	3.66	6.11	14.4	6.5
^{140}Ce	380	47.5	138	2.20	3.54	5.39	12.6	5.7
^{208}Pb	85.5	40.3	266	3.24	6.85	8.14	11.0	3.7

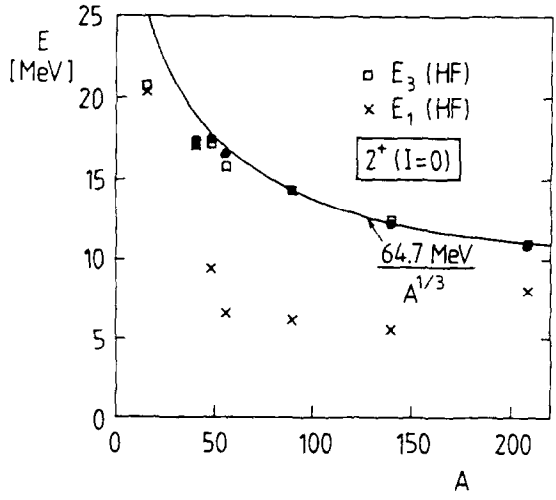

FIG. 7. Energies E_3 (squares) and E_1 (crosses) evaluated for the quadrupole operator (3.8) with the SkM* force. Experimental points from Ref. [5] (shown by heavy dots, their size indicating the error bars). Solid line: Eq. (3.9).

moment m_k. This dependence is explicitly recognized from Eqs. (A.61) and (A.62) for m_1 and m_3, respectively. The polarisability m_{-1} is inversely proportional to a stiffness, i.e., a second derivative of the total energy with respect to the quadrupole moment, and thus goes like $A^{7/3}$. Now, for m_{-3} one knows [62] that the mass parameter goes like $A^{-5/3}$ in the scaling limit. Since such a mass parameter in the adiabatic case is proportional to $m_{-3}/(m_{-1})^2$, it follows that m_{-3} scales as A^3.

From Table VII and Fig. 7, one sees that m_3 and m_1 follow pretty well this general A-dependence. This is hardly the case for m_{-1} and even less for m_{-3}, at least for nuclei which are not spin-saturated (as, e.g., ^{48}Ca or ^{56}Ni, where the $1f_{7/3}$ subshell is filled but not its spin-orbit partner). For the latter, low-energy ($0\hbar\omega$) excitations coexist with $2\hbar\omega$ excitations of a giant resonance character, whereas the low-energy component is suppressed by the Pauli principle in spin-saturated nuclei (as, e.g., ^{16}O or ^{40}Ca). The resulting strength distribution is thus much more spread for not spin-saturated nuclei towards low excitation energies. The effect of such a spreading is of course more noticeable in m_{-3} (or m_{-1}) than in m_3 (or m_1). Upon increasing A, the intrusion of more and more high-j subshells into lower shells washes out the distinction between 0 and $2\hbar\omega$ excitations, reducing therefore the fluctuations with A of, e.g., the adiabatic mass parameter. (See the discussion of Ref. [34].)

The above discussion illustrates on one particular example the fact that the density variational formalism mostly used in this paper is well suited for physical situations, where shell effects do not play any important role, and should otherwise be supplemented by an explicit account of quantal properties.

In Table VII the upper bound $\sigma_{\max}$ for the variance, defined in Eq. (2.13), is also given. Since this quantity incluces E_1 (and thus m_{-1}), one finds fluctuations in $\sigma_{\max}$

reflecting those of m_{-1}. For the quadrupole mode, the connection of the quantity $\sigma_{\max}$ as defined in Eq. (2.13) with the width of the giant resonance is, however, meaningless in those nuclei where an appreciable amount of the quadrupole strength is found in the low-lying ($0\hbar\omega$) vibrations so that the strength function no longer exhibits a single peak.

The separate variation of E_3 and E_1 with A is displayed on Fig. 7. One retrieves, as expected for this mode, the approximate $A^{-1/3}$ dependence of E_3 (as well as of E_1 up to the above-discussed shell fluctuations). On this figure also, experimental GQR energies E_Q are reported (for references, see the compilation of Speth and van der Woude [5]). Our calculated E_3 values fall in most cases within the error bars. In Ref. [5], the following parametrisation of E_Q, extracted from Ref. [22],

$$E_Q = 64.7A^{-1/3}\ \text{MeV} \tag{3.9}$$

has been deemed as providing a good reproduction of data for nuclei with $A > 90$; it is shown in Figs. 7 and 8 by a solid line. From a least-squares fit to our results with the force SkM*, we find for the coefficient in Eq. (3.9) rather the value 64.9 MeV.

In Fig. 8 we compare the energies E_3 obtained for a series of Skyrme forces. The variation is seen not to be very large. This is due to the fact that more than 95 % of the moment m_3 is coming from the kinetic and the effective mass terms, whereas Coulomb, spin-orbit and finite-range terms contribute less than 5 % (see also Ref. [6]). The energy E_3 for the GQR thus depends on the interaction only through the effective mass which can roughly be characterized by its value m^*_∞ for infinite nuclear matter, a value which is quite similar in all Skyrme forces used here (see

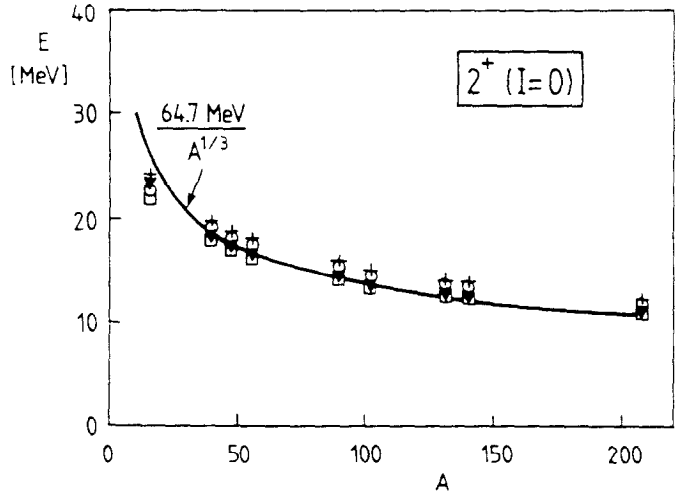

FIG. 8. Energies E_3 for the GQR, evaluated for various Skyrme forces: SkM* (squares), Ska (crosses), RATP (circles), and SIII (triangles). Solid line: Eq. (3.9), representing the experimental peak values.

Table IX). (A very weak force dependence also comes, in principle, through the moment m_1 which is proportional to the mean squared radius and thus fitted to be roughly the same for the different forces.)

We finally point out that the isotopic variation of the GQR energy for Sn isotopes has recently been measured carefully [93]. As seen on Fig. 4 in Section 3.1 above, our calculated E_3 energies reproduce extremely well also these data. Such results (variation of E_3 with A as well as with the neutron number N) confirm the relevance of SkM* force also for the description of the GQR properties.

The good fit of the force SkM* is no big surprise since this force differs only in the finite-range term E_{fin} in (A.42) from the force SkM which was originally adjusted to the GQR (and GMR) energies [58]; in particular, the two forces have exactly the same infinite matter properties including m^*_∞ (see Table IX).

3.4. *Giant Octupole Resonances*

Up to now there is not much experimental knowledge about the isoscalar octupole ($I=0$, $J\pi=3^-$) giant resonance. The relative strength of the low multipolarity modes even in the region of ~ 100 MeV $A^{-1/3}$ is still so large that octupole and higher modes are difficult to be clearly detected. Nevertheless there are clear indications that a substantial amount of octupole m_1 strength is found in the region of $3\hbar\omega$ excitations in several nuclei; for a discussion of the experimental evidence we refer to the review of Bertrand [112]. It is therefore of some interest also to give theoretical predictions where the octupole giant resonance should be expected. (See also the fluid dynamical calculations in Ref. [113].)

In our scheme we use the operator

$$\hat{Q} = r^3 P_3(\cos\vartheta) = z^3 - \tfrac{3}{2} z(x^2 + y^2) \tag{3.10}$$

to create a collective octupole vibration. With this operator it is, although straightforward, a rather lengthy algebraic task to evaluate the commutators for the m_3 sum rule. The formulae for m_1 and m_3 are given in the Appendices 2.6 and 3. Combinings Eqs. (A.69) and (A.77), we obtain for spherical nuclei in the semiclassical (ETF) approximation the following contribution of the kinetic and effective mass terms to the m_3 moment,

$$m_3^{\text{kin}} + m_3^{\text{eff}} = \frac{1}{4}\left(\frac{\hbar^2}{m}\right)^3 \sum_q \int d^3r f_q(r)[40r^2\tau_q(r) - 15\rho_q(r)], \tag{3.11}$$

where $f_q(r) = m/m^*_q(r)$ contains the effective mass [56]. (The derivation of Eq. (3.11) involves a semiclassical density matrix expansion for the evaluation of the single-particle angular momentum density, given in Appendix 3.) As in the case of the quadrupole giant resonance, the kinetic and effective mass contributions to m_3 are the leading ones. Coulomb and finite-range contributions (given in Eqs. (A.70), (A.71)) give 14 % (in Ca) to 7 % (in Pb) to the total m_3; they would be partially cancelled by the spin-orbit contributions which were neglected here.

In Fig. 9 we give the numerical results for the E_3 energies, obtained both microscopically (HF, with Eq. (A.69)) and semiclassically, i.e., using the ETF functional $\tau[\rho]$ in Eq. (3.11). As in the case of the quadrupole mode, the energy E_3 is not suited to represent the low-lying collective octupole strength due to $1\hbar\omega$ particle-hole excitations. The latter might, however, slightly reduce the E_3 values with respect to the experimental average energies of the high-lying strength.

It is worth noting that for a spherical nucleus we have no problems with the spurious center of mass motion. (This would lead to an isoscalar dipole contribution to the mode, which would have to be explicitly substracted.) To demonstrate this, we evaluate the center of mass $z(\alpha)$ of the scaled density:

$$z(\alpha) = \frac{1}{A}\int \rho_0(\mathbf{r})\, e^{\alpha \hat{S}_3} z\, d^3r$$

$$= -\frac{3}{A}\frac{\hbar^2}{m}\langle 0|\, \alpha \hat{Q}_{20}\left[1 + 9\left(\frac{\hbar^2}{m}\right)^2 \alpha^2 z^2\right]|0\rangle + O(\alpha^5). \tag{3.12}$$

In the case of spherical symmetry, where $\langle z^2\rangle = \frac{1}{3}\langle r^2\rangle$ and the quadrupole moment $\langle \hat{Q}_{20}\rangle$ is zero, this yields

$$z(\alpha) = -\frac{18}{5}\left(\frac{\hbar^2}{m}\right)^3 \langle r^4\rangle \alpha^3 + O(\alpha^5) \tag{3.13}$$

and, therefore, we get the center of mass contribution to the collective kinetic energy

$$K_{CM}(\alpha, \dot{\alpha}) = \frac{M}{2}\dot{z}^2(\alpha) = \frac{324}{25}\left(\frac{\hbar^2}{m}\right)^6 \langle r^4\rangle^2 \alpha^4 \dot{\alpha}^2 = 0 \qquad (\text{at } \alpha = 0). \tag{3.14}$$

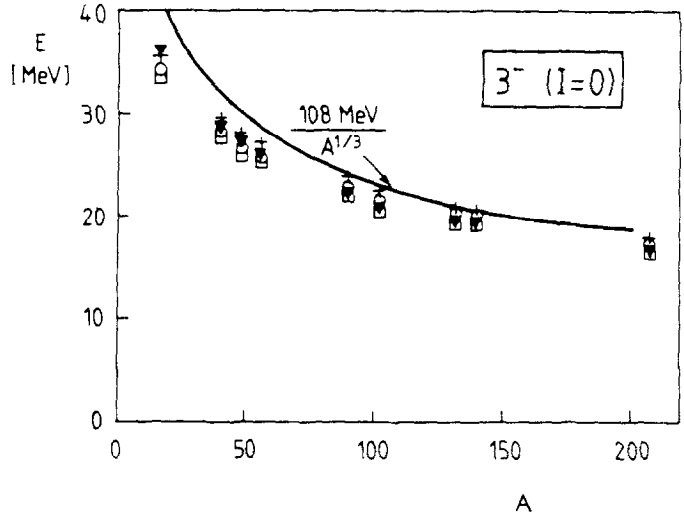

FIG. 9. Giant octupole resonance energies E_3 for spherical nuclei, obtained with four different Skyrme forces (symbols as in Fig. 8). The solid line gives a fit to the experimental values [5, 112, 114].

In a deformed nucleus with nonzero quadrupole moment $\langle \hat{Q}_{20} \rangle$, the leading term of the center of mass contribution to the collective kinetic energy is then

$$K_{CM}(\dot{\alpha}) = \frac{1}{2} \left(\frac{\hbar^2}{m} \right)^2 \frac{9m}{A} \langle \hat{Q}_{20} \rangle^2 \dot{\alpha}^2. \tag{3.15}$$

This has to be added to $\frac{1}{2} B_\alpha \dot{\alpha}^2 = \frac{1}{2} (\hbar^2/m)^2 \, 3mA \langle r^4 \rangle \dot{\alpha}^2$, see Eq. (A.64), leading thus to an increased inertial parameter B_α. An estimation with typical quadrupole moments for rare-earth nuclei leads to an increase of B_α of 10 to 15 %.

3.5. *Temperature Dependence of Giant Resonance Properties*

As already discussed in the Introduction and in more detail in Section 2.2, it is of interest to investigate the giant resonances of highly excited nuclei in the statistical approximation. We refer to that section for the finite-temperature formalism and just recall here that we treat the giant resonances as fast diabatic, *isentropic* vibrations around a thermodynamically equilibrated ground state at given temperature T.

A few remarks are appropriate about the parametrisation of the trial nuclear densities at finite temperature. Since an excited nucleus above nucleon evaporation threshold is not stable, an artificial device has to be invented in the theoretical calculations in order to treat it by a static variational principle such as the HF or the density variational method. One procedure, advocated by Bonche and collaborators [115, 116], is to embed the nucleus in a background nucleon gas at thermodynamical equilibrium and to extract its thermal properties from the variational solution by subtracting the background gas part of the corresponding grand potential. Another procedure, treating the nucleus explicitly as a mestastable system [117], consists in including it in a box of finite radius and imposing zero external pressure by suitable boundary conditions [118, 119]. A careful comparison and discussion of the two procedures and their effects on the giant resonances at finite temperatures is published elsewhere [119].

In our present work, we chose the somewhat more convenient approach to neglect the effect of any external nucleon gas and thus to force the variational densities to go to zero in the outer surface as in Eq. (2.36), even at finite temperatures (see also Refs. [10, 46, 47, 72, 109]). This corresponds, on the microscopic level, to the neglect of the higher continuum states of the nucleons in HF calculations [39], which was shown [115] to be a good approximation up to temperatures of $\simeq 4$ MeV. We shall therefore not exceed a limit of 4-MeV temperature in our calculations. To the extent that our results presented below are very similar to those of a calculation [120] where the subtraction procedure of Bonche *et al.* was used, we can expect that they do not depend crucially on a more sophisticated density parametrisation.

In the following we shall present a few selected results of GR energies and sum rules as functions of the temperature T.

In Fig. 10 we present various GR energies of the nucleus ^{208}Pb as functions of the temperature T, evaluated with the SkM* force (see the detailed explanation in the figure caption). They are seen to vary very little (or not at all, in the case of the 2^+ mode), except for the isovector monopole (0^+, $I=1$) case. The constancy of the GQR energy is not the result of a cancellation; the sum rule m_3 is decreasing and the sum rule m_1 (i.e., the r.m.s. radius) is increasing with temperature, but these variations are both very small. The decrease of the GMR (0^+) E_1 energies is mainly due to an increase of the monopole polarisabilities (i.e., m_{-1}) with increasing T, in particular, in the isovector case.

Similar results are shown in Fig. 11 for the nucleus ^{40}Ca. The decrease of the monopole GR energies with increasing temperature is stronger here than in Pb, which explains itself by the fact that this nucleus "consists" mainly of surface and thus is softer. (The decrease of the finite-nucleus incompressibility K_A—see Fig. 12 below—is stronger than that of saturated (infinite) nuclear matter which dominates

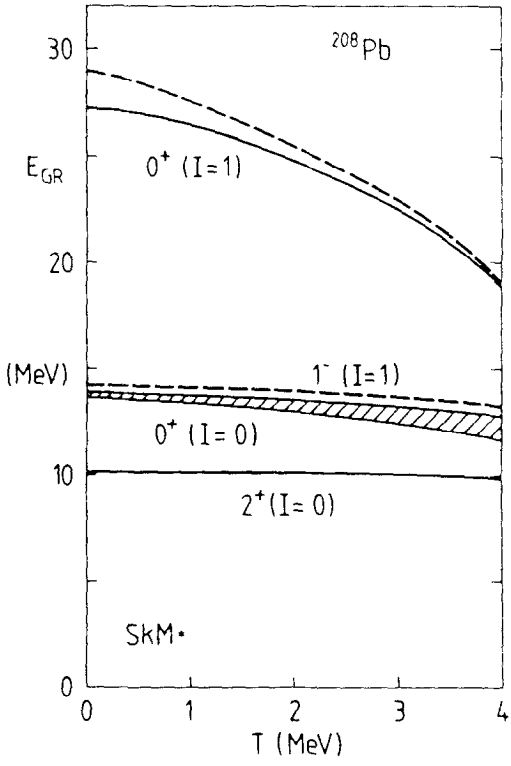

FIG. 10. GR energies for the ^{208}Pb nucleus, obtained with the SkM* force. Solid lines: HF, dashed lines: ETF density variational results. $0^+(I=0)$: E_3 (upper line) and E_1 (lower line) with operator (A.42). The difference (shaded area) is a measure for the width (see Eq. (2.11)). $0^+(I=1)$: energy E_1 including κ_1 using operator (A.47). Note the decrease of the shell effect (difference between solid and dashed lines) with increasing temperature. $1^-(I=1)$: energy E_1 including κ_1 using operator (A.54) (see Ref. [47] for details). $2^+(I=0)$: energy E_3 with operator (A.59).

the Pb nucleus.) We have also included here the energy E_3 for the octupole GR ($3^-, I=0$). It shows a somewhat strange bump, although very weak, as a function of temperature. This variation is not a shell effect, since the HF and semiclassical results here agree within less than a few hundred kilo electron volts. It was also observed in Ref. [50]. The GDR energies ($1^-, I=1$) are not shown here; they lie within a million electron volts of the GQR ($2^+, I=0$) energies and have the same weak temperature variation as in the case of ^{208}Pb seen in Fig. 10.

The increasing discrepancies between HF and semiclassical energies, seen for the monopole (0^+) modes at temperatures higher than 3 MeV, must be ascribed to the truncation of the single-particle level spectrum used in the HF code which is, in fact, too restricted at these temperatures in this light nucleus. A more rigorous numerical treatment of the continuum states, as, e.g., done in Ref. [115], would be appropriate here.

An interesting quantity is the incompressibility K_A^{scal}, which is proportional to

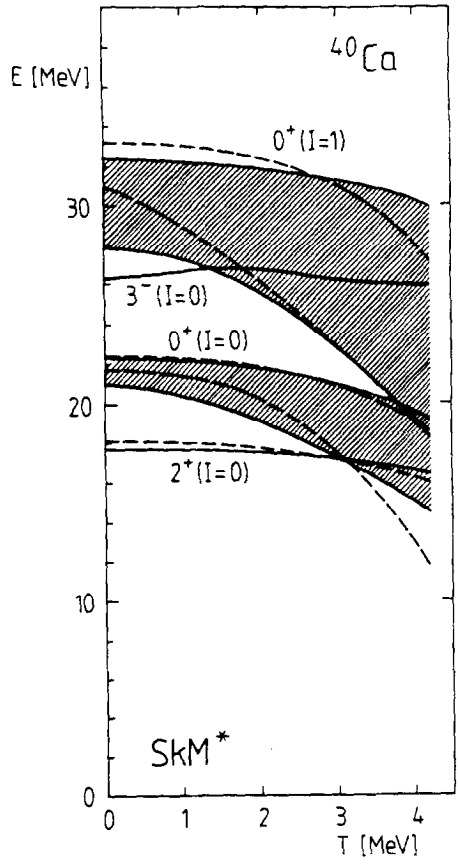

FIG. 11. Same as in Fig. 10, but for the ^{40}Ca nucleus. $3^-(I=0)$: energy E_3 with operator (A.63). For the isovector GMR ($0^+, I=1$), also the energy E_3 is shown and connected to E_1 by the dashed lines.

m_3, see Eq. (A.46). It is shown as a function of temperature for two nuclei in Fig. 12. The decrease of this quantity from $T=0$ to 4 MeV—13 % in Pb and 17 % in Ca—is stronger than that of the infinite nuclear matter incompressibility K_∞ (which is of 9 % only [10, 121]). This increased temperature effect can be understood in terms of a "leptodermous" or liquid drop model type expansion of K_A^{scal} [10, 122]. The leading (or volume) term of K_A^{scal} is K_∞ which for the SkM* force equals 217 MeV at $T=0$ (see Table IX in the Appendix). The surface correction is strongly negative and reduces it (apart from Coulomb, curvature, and asymmetry effects) to values around 140 MeV at $T=0$. This negative surface contribution is increasing with temperature as the surface of the nucleus becomes more diffuse and has, therefore, a larger effect in Ca than in Pb.

Unfortunately, it is difficult to directly compare our calculated variation of the GDR energy with the experimental one [36, 37], due to deformation and rotational effects and the associated error bars. An assessment of such a variation (or, possibly, the variation or constancy of other GR energies) would yield a very important constraint on the nuclear equation of state in the low-temperature range considered here. The latter plays an important role in model calculations of a supernova explosion (see, e.g., Refs. [123, 124]), in particular, through the value of the nuclear matter incompressibility K_∞.

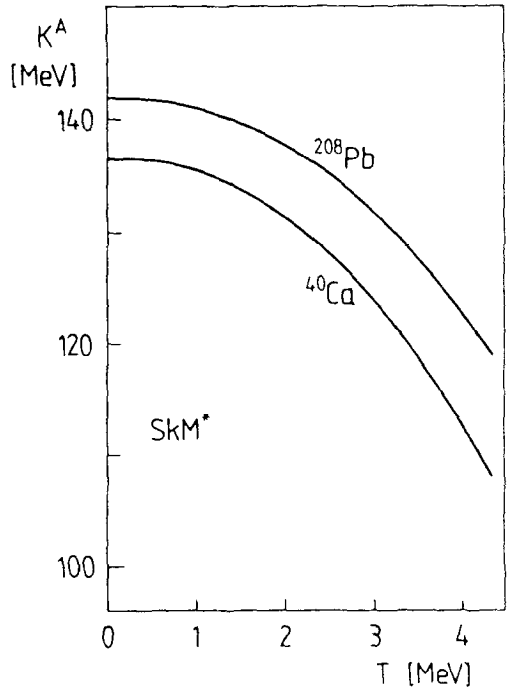

FIG. 12. Incompressibility K_A^{scal} (A.46) of the nuclei ^{208}Pb and ^{40}Ca, obtained with the SkM* force, versus temperature T.

Throughout this paper, we have neglected the pairing interactions. In the context of the present discussion of temperature dependences, the question arises how a phase transition from paired to normal state could affect the properties of the giant resonances discussed here. Within the crude BCS approximation, such a phase transition is expected around temperatures of 0.5–1 MeV for infinite nuclear matter. For finite nuclei it is clear that a sharp phase transition cannot occur in a more appropriate treatment of pairing correlations which one then expects to disappear slowly with increasing temperature. It has, indeed, been shown [125] how thermal fluctuations together with a proper account of spurious particle number fluctuations wash out a sharp phase transitions. The GDR of the nucleus ^{58}Ni has been studied recently in the finite-temperature RPA framework [126]. It was found that the inclusion of thermal fluctuations and a removal of particle number fluctuations lead to a very weak temperature dependence of the centroid energy $\bar{E}$ of the GDR, such that the latter can be obtained in a good approximation using simply the ground-state pairing gap Δ ($T=0$) at all temperatures. Knowing that the GR energy positions are very little affected by pairing effects at zero temperature (see, e.g., Ref. [31]), we may thus conclude that the picture which we have obtained in the present studies would not be changed appreciably by the proper inclusion of pairing correlations.

4. Summary and Conclusions

We have presented a consistent density variational approach to the study of electric giant resonances, both isoscalar and isovector, of spherical nuclei. We start from a microscopic RPA sum rule description which takes full advantage of the simple analytical form of the effective nucleon–nucleon interaction in use here, namely the Skyrme force. We obtain variational solutions for the nuclear ground state through a minimisation of the total (free) energy in a suitably chosen space of (local) trial densities, employing the gradient expansion of the total energy density functional within the extended Thomas–Fermi framework up to fourth order in $\hbar$. From these static equilibrium densities we then calculate the dynamical quantities required for the description of the giant resonances, namely the first and third moments (m_1 and m_3, respectively) of the strength functions associated to the chosen excitation operators.

As a result of our calculations, the moments m_1 and m_3 are shown to be practically unaffected by shell effects; the quantitative agreement between semiclassical and microscopical Hartree–Fock results for these moments provides a nice justification of the semiclassical approximation used here. In the lower order moments, however, shell effects do in general play an important role. For isoscalar quadrupole deformations, the availability of Hartree–Fock codes for both potential energy surfaces and adiabatic mass parameters has led us to evaluate also the moments m_{-1} and m_{-3} incorporating the required shell effects.

Throughout this work we have used the SkM* parametrisation of the effective Skyrme force [10, 57]. In some cases, however, other parametrizations have been employed for the sake of a systematical comparison. The SkM* force, shown to yield good saturation and surface properties within the whole stability valley, appears from the present results to be rather well suited also for the description of harmonic collective modes, as will be briefly summarized.

In the monopole modes (both isoscalar and isovector), the correct reproduction of the experimental giant resonance energies in light nuclei requires a description of the collective vibration in terms of more than a single scaling mode. Two modes have been considered which correspond to bulk and surface breathing vibrations. By coupling these two modes we reproduce correctly the A-dependence of the measured breathing mode energies as well as the fact that in light nuclei half (or more) of the isoscalar monopole strength is missing in the observed 0^+ ($I=0$) states. *Within the family of Skyrme forces considered and the Hartree–Fock + RPA framework used here*, we confirm the earlier result [30] that the experimental breathing mode energies are only compatible with forces whose values of the nuclear bulk incompressibility K_∞ are inferior to 230–250 MeV. However, even in the best fit, obtained with the SkM* force, there is a systematic discrepancy between calculated and experimental GMR energies of about 1 MeV in medium nuclei and ~ 2 MeV, on the average, in light nuclei.

An attempt was recently made [96] to fit the newest precision data [93] of GMR energies by Eq. (3.3), using experimental values of $\langle r^2 \rangle$ and a LDM type expansion of the incompressibility K_A of the form $K_A = K_\infty + K_S A^{-1/3} + (\text{higher order terms})$. The best fits were obtained with the values $K_\infty \simeq (300 \pm 25)$ MeV and $K_S \simeq (-750 \pm 80)$ MeV. To the extent that K_∞ might be identified with the infinite-nuclear-matter incompressibility $K_{\infty,\infty}$, this seems to call for a new determination of Skyrme forces. Such an identification depends, however, on the particular dynamics of the nuclear breathing mode, as discussed in the beginning of Section 3.1.1. In the case of scaling (described by the excitation operator r^2), $K_\infty = K_{\infty,\infty}$. But in the same limit, most Skyrme forces were found [91, 122] to have approximately $K_S \sim -K_{\infty,\infty}$. The above empirical values thus indicate that the breathing mode in nature does not follow the scaling dynamics (as is the case also in our 2-dimensional hydrodynamical model in Section 3.1.1) which, in turn, puts in cause the assumption that $K_\infty = K_{\infty,\infty}$. The results of Ref. [96] are therefore not in contradiction with our findings using the conventional family of Skyrme forces. They rather represent a phenomenological parametrization of breathing mode energies which implies that, if one takes the newest experimental data very literally, the last word about the nuclear incompressibility $K_{\infty,\infty}$ has not been told yet.

For the isovector dipole mode, where extensive information on the relevant strength function is available, we reproduce rather well the experimental m_{-1} moments; also the obtained m_1 moments are qualitatively consistent with experimental findings. Using, again, a two-dimensional description by coupling surface (Goldhaber–Teller) and volume (Migdal) dipole oscillations, we reproduce very well the average A-dependence of the experimental GDR energies, hereby

showing evidence that the volume (Migdal) mode becomes more and more important upon increasing the nucleon number. The question to which extent the Hartree–Fock approach (and *a fortiori* its semiclassical alternative) should reproduce the enhancement factor beyond the Thomas–Reiche–Kuhn sum rule remains, however, open.

The experimental energies of the (isoscalar) giant quadrupole resonances are very well reproduced by our calculated E_3 energies, also for a series of recently measured Sn isotopes. Shell effects in the moments m_{-1} (or m_{-3}, respectively) result in large deviations with respect to the $A^{7/3}$ (or A^3, respectively) bulk variation for a A-nucleon system.

Although not much systematic experimental evidence is available on the high-lying, giant resonance type ($I=0$) octupole strength, we have calculated the energies E_3 also for this mode.

Our approach has been generalized and applied to the finite temperature case, or more specifically, to excited nuclei. Since for giant resonance modes it is likely that one is dealing with a fast diabatic process, one has to scale the wave functions with *fixed* fermion occupation probabilities in evaluating m_1 and m_3 moments, which clearly leads to an isentropic motion which is not quasi-static. We find that the temperature variation of the giant resonance energies is, in general, rather weak.

The limitations of the present studies are twofold: they deal only with electric modes and they concern only spherical nuclei. Work is currently under progress to extend this approach to deformed nuclei [98]. A corresponding study of magnetic modes would be very valuable and timely for the purpose of determining more accurately the relevant components of the Skyrme effective force, which still are rather poorly known. (See, however, Ref. [60].)

As discussed in Section 2.3, our method has much in common with the so-called fluid-dynamical approach [19–23, 65–69, 107]. We have, however, the advantage of dealing with realistic smooth density profiles instead of step functions and of being capable to include also the nonlocal parts of the effective nuclear force, i.e., spin-orbit and effective mass terms, and the Coulomb interaction. As a possible drawback one might take the fact that, at present, the eigenmodes for a given multipolarity have to be guessed in the form of the excitation operators $\hat{Q}$ (or the corresponding velocity fields $\mathbf{u}$), even though a lot can be gained here by using physical intuition. On the other hand, the "coupled-modes" extension of the scaling approach, which we used successfully in the monopole and the dipole cases, can be taken as a first step towards a more general and systematic variation and/or coupling of various operators (or velocity fields) which generate a RPA-like spectrum [134]. It might be interesting to note that such an approach, combined with the semiclassical density variational method, has recently been shown to be well suited for the description of collective excitations of the electrons in metal clusters [127, 134].

It is interesting also to compare our results for the RPA moments m_k obtained for the isoscalar 0^+ and 2^+ modes for light nuclei with those of generator coordinate method calculations [28] with the same for SkM*. In the case of the breathing mode of ^{40}Ca (see our results given in Table II of Section 3.1), the m_{-1} values

agree within 5%, but the m_1 values are at variance by $\sim 13\%$. This most likely reflects the rather limited character of the variational space used in Ref. [28], preventing thus a more accurate prediction of m_k moments with $k > 0$. As to the quadrupole mode for which our results are shown in Table VII of Section 3.3, the values of the moments m_{-3} and m_{-1} obtained in the two approaches for the nuclei ^{16}O and ^{40}Ca agree within an error margin of 2–4% The m_1 values, however, disagree by $\sim 10\%$, similarly to the monopole case, and the m_3 values even more.

It was not the purpose of the present paper to present a systematic analysis of all the detailed experimental data which today are available on nuclear giant resonances. We rather wanted to illustrate our semiclassical RPA sum rule approach by way of typical examples for the most prominent modes. More detailed analyses and extensions to deformed nuclei and to other spin–isospin modes have been left to a future work. Nevertheless, it seems clear already that this approach using the SkM* Skyrme force does reproduce in a satisfactory way the main trends of observed giant resonance energies for both isovector and isoscalar electric modes.

APPENDIX 1: Scaling Approach to Isoscalar Modes

1.1. *One-Dimensional Case*

Assume that for a given Hamiltonian with kinetic energy $\hat{T}$ and potential energy $\hat{V}$

$$\hat{H} = \hat{T} + \hat{V} = \sum_{i=1}^{A} \hat{t}(i) + \sum_{i<j}^{A} \hat{V}(i, j) \tag{A.1}$$

one has

$$[\hat{H}, \hat{Q}] = [\hat{T}, \hat{Q}], \tag{A.2}$$

i.e., the operator $\hat{Q}$ commutes with the potential energy. This holds for *isoscalar*, *local* operators $\hat{Q}$ in connection with Skyrme forces [6, 34]. The moments m_3 and m_1 defined in Eqs. (2.3a) and (2.3b) then have a simple physical meaning, as we shall see. We first define the scaling operator $\hat{S}$ by

$$\hat{S} = [\hat{T}, \hat{Q}] = \tfrac{1}{2}(\nabla \cdot \mathbf{u}) + \mathbf{u} \cdot \nabla, \tag{A.3}$$

where

$$\mathbf{u}(\mathbf{r}) = -\frac{\hbar^2}{m} \nabla Q(\mathbf{r}). \tag{A.4}$$

The operator $\hat{S}$ creates a deformed (or scaled) state by means of a unitary transformation of the HF ground state:

$$|\alpha\rangle = e^{-\alpha \hat{S}} |0\rangle. \tag{A.5}$$

Hereby the *real* variable α is called scaling parameter and is understood as a collective variable $\alpha(t)$. The time-dependent one-body density is then

$$\rho(\mathbf{r}, t) = \rho(\mathbf{r}, \alpha(t)) = \sum_{i=1}^{A} |\varphi_i(\mathbf{r}, \alpha)|^2 = e^{-\alpha((\nabla \cdot \mathbf{u}) + \mathbf{u} \cdot \nabla)} \rho(\mathbf{r}), \tag{A.6}$$

where $\varphi_i(\mathbf{r}, \alpha)$ are the scaled HF single particle wavefunctions[6]:

$$\varphi_i(\mathbf{r}, \alpha) = e^{-\alpha \hat{S}} \varphi_i(\mathbf{r}) \tag{A.7}$$

and $\rho(\mathbf{r})$ is the density of the HF ground state. One immediately sees now that

$$\frac{\partial}{\partial \alpha} \rho(\mathbf{r}, \alpha) = -\nabla \cdot (\rho \mathbf{u}), \tag{A.8}$$

so that $\mathbf{u}(\mathbf{r})$ is recognized as a displacement field defining a velocity field

$$\mathbf{v}(\mathbf{r}, t) = \dot{\alpha}(t)\, \mathbf{u}(\mathbf{r}), \tag{A.9}$$

which satisfies the continuity equation

$$\frac{\partial \rho}{\partial t} + \nabla \cdot (\rho \mathbf{v}) = 0. \tag{A.10}$$

From Eq. (A.3) one then sees that the moment m_1^{RPA} is proportional to the hydrodynamical inertial parameter B_α at the ground state ($\alpha = 0$):

$$m_1^{\mathrm{RPA}} = \frac{1}{2\hbar^2} B_\alpha; \qquad B_\alpha = m \int \mathbf{u}^2(\mathbf{r})\, \rho(\mathbf{r})\, d^3r. \tag{A.11}$$

It is interesting to note that for the particular scaling dynamics described here, B_α is also identical to the cranking (or Inglis) inertia (see Ref. [64])

$$B_\alpha^{\mathrm{cr}} = 2\hbar^2 \sum_{n>0} \frac{\left| \langle n | \dfrac{\partial}{\partial \alpha} | 0 \rangle \right|^2}{E_n - E_0} = B_\alpha = 2\hbar^2 m_1^{\mathrm{RPA}}. \tag{A.12}$$

Due to Eq. (A.5), the moment m_3^{RPA} is seen to be one-half of the harmonic oscillator stiffness parameter C_α of the scaled HF energy:

$$m_3^{\mathrm{RPA}} = \frac{1}{2} \langle 0 | [\hat{S}, [\hat{S}, \hat{H}]] | 0 \rangle = \frac{1}{2} \frac{d^2}{d\alpha^2} [\langle \alpha | \hat{H} | \alpha \rangle]_{\alpha = 0} = \frac{1}{2} C_\alpha. \tag{A.13}$$

[6] For simplicity we shall use one and the same symbol for a one-body operator whether it acts on a single-particle wavefunction or on a Slater determinant of the A-particle system.

Thus, the energy E_3 in Eq. (2.8) is equal to the first vibrational excitation energy of the collective Hamiltonian

$$\hat{H}_{\text{coll}}(\alpha) = \tfrac{1}{2}B_\alpha \dot{\alpha}^2 + \langle \alpha | \hat{H} | \alpha \rangle \tag{A.14}$$

in the harmonic approximation:

$$E_3 = \sqrt{m_3^{\text{RPA}}/m_1^{\text{RPA}}} = \hbar \sqrt{C_\alpha / B_\alpha} = \hbar\omega_\alpha. \tag{A.15}$$

1.2. *Multidimensional Modes*

The scaling approach is easily generalized to the case of several collective scaling variables. Let us assume that one starts from a set of variables $\boldsymbol{\alpha} = \{\alpha_i(t)\}_{(i=1,2,\ldots,M)}$ and corresponding displacement fields $\mathbf{u}_i(\mathbf{r})$ such that

$$\rho(\mathbf{r}, t) = \rho(\mathbf{r}, \boldsymbol{\alpha}(t)), \tag{A.16}$$

$$\frac{\partial \rho}{\partial \alpha_i} + \nabla \cdot (\rho \mathbf{u}_i) = 0. \tag{A.17}$$

One may define accordingly the scaling operators

$$\hat{S}_i = \tfrac{1}{2}(\nabla \cdot \mathbf{u}_i) + \mathbf{u}_i \cdot \nabla \tag{A.18}$$

which create multidimensionally "deformed" Slater determinants $|\boldsymbol{\alpha}\rangle$:

$$|\boldsymbol{\alpha}\rangle = \prod_{i=1}^{M} e^{\alpha_i \hat{S}_i} |0\rangle. \tag{A.19}$$

The collective potential energy then will be

$$V_{\text{coll}}(\boldsymbol{\alpha}) = \langle \boldsymbol{\alpha} | \hat{H} | \boldsymbol{\alpha} \rangle \tag{A.20}$$

and the stiffness tensor C_{ij} is defined by

$$C_{ij} = \left[\frac{\partial^2}{\partial \alpha_i \, \partial \alpha_j} \langle \boldsymbol{\alpha} | \hat{H} | \boldsymbol{\alpha} \rangle \right]_{\boldsymbol{\alpha}=0} = \langle 0 | [\hat{S}_i, [\hat{S}_j, \hat{H}]] | 0 \rangle. \tag{A.21}$$

(Note that, even though the $\hat{S}_i$ may not commute amongst each other, C_{ij} is symmetric if $|0\rangle$ is the HF ground state of $\hat{H}$.) The inertial tensor B_{ij} is straightforwardly found from the velocity fields $\mathbf{u}_i$,

$$B_{ij} = m \int \mathbf{u}_i(\mathbf{r}) \cdot \mathbf{u}_j(\mathbf{r}) \, \rho(\mathbf{r}) \, d^3r, \tag{A.22}$$

so that the collective Hamiltonian in the harmonic approximation is

$$\hat{H}_{\text{coll}}(\{\alpha_i\}) = \frac{1}{2} \sum_{i,j=1}^{M} B_{ij} \dot{\alpha}_i \dot{\alpha}_j + \frac{1}{2} \sum_{i,j=1}^{M} C_{ij} \alpha_i \alpha_j. \tag{A.23}$$

From the system of M coupled oscillators (A.23), one finds M eigenmodes with frequencies ω_n and eigenvectors x_j^n by solving the secular equations,

$$\sum_{j=1}^{M} (C_{ij} - \omega_n^2 B_{ij}) x_j^n = 0 \qquad (i, n = 1, ..., M), \tag{A.24}$$

which is equivalent to diagonalizing the matrix $(B^{-1}C)_{ij}$. The corresponding unitary transformation matrix U_{ij} and its transposed matrix U_{ij}^t then define some diagonal matrices $\tilde{C}$ and $\tilde{B}$ by

$$\tilde{C}_{ij} = (U^t C U)_{ij} = \tilde{C}_i \delta_{ij}, \qquad \tilde{B}_{ij} = (U^t B U)_{ij} = \tilde{B}_i \delta_{ij}, \tag{A.25}$$

so that

$$\omega_i = \sqrt{\tilde{C}_i / \tilde{B}_i}. \tag{A.26}$$

From now on, $\mathbf{u}_i$ shall be the velocity fields of the eigenmodes fulfilling the orthogonality relation

$$\int \mathbf{u}_i \cdot \mathbf{u}_j \rho(\mathbf{r})\, d^3r = \frac{\tilde{B}_i}{m} \delta_{ij}. \tag{A.27}$$

We shall now prove some restricted sum rules. Let $\hat{Q} = Q(\mathbf{r})$ be a local, spin- and isospin-independent operator whose gradient lies in the space spanned by the $\mathbf{u}_i$, so that

$$\nabla Q = \sum_{i=1}^{M} a_i \mathbf{u}_i \tag{A.28}$$

with

$$a_i = \frac{m}{\tilde{B}_i} \int (\nabla Q) \cdot \mathbf{u}_i \rho\, d^3r. \tag{A.29}$$

The squared transition matrix elements of Q from the ground state to the one-phonon state $|i\rangle$ (with energy $\hbar\omega_i$) can be shown in the semiclassical limit to be [68]

$$|\langle i|\, Q\, |0\rangle|_{sc}^2 = \frac{\hbar}{2\omega_i \tilde{B}_i} \left| \int Q\, \delta\rho_i\, d^3r \right|^2, \tag{A.30}$$

where $\delta\rho_i$ is the transition density

$$\delta\rho_i = \frac{\partial \rho}{\partial \alpha_i} = -\nabla \cdot (\rho \mathbf{u}_i). \tag{A.31}$$

Using Eqs. (A.28) and (A.30) one gets, after a partial integration,

$$|\langle i|\, Q\, |0\rangle|^2_{sc} = \frac{\hbar \tilde{B}_i a_i^2}{2m^2 \omega_i}. \tag{A.32}$$

With this, the energy-weighted sum rule contribution of the one-phonon states is

$$m_1(Q) = \sum_{i=1}^{M} \hbar\omega_i\, |\langle i|\, Q\, |0\rangle|^2_{sc} = \frac{\hbar^2}{2m^2} \sum_{i=1}^{M} a_i^2\, \tilde{B}_i. \tag{A.33}$$

On the other hand, with Eqs. (A.11), (A.27), and (A.28) one finds

$$\begin{aligned} \frac{1}{2}\langle 0|\, [Q, [\hat{H}, Q]]\, |0\rangle &= \frac{1}{2}\langle 0|\, [Q, [\hat{T}, Q]]\, |0\rangle \\ &= \frac{\hbar^2}{2m} \int \rho (\nabla Q)^2\, d^2 r = \frac{\hbar^2}{2m^2} \sum_{i=1}^{M} a_i^2 \tilde{B}_i. \end{aligned} \tag{A.34}$$

Comparing Eqs. (A.34) and (A.33) we see that the m_1 sum rule of an operator fulfilling Eq. (A.28) is exhausted by the one-phonon states corresponding to the M eigenmodes $\mathbf{u}_i$ (see also Ref. [128]). Similarly, we find that the cubic-energy weighted sum rule for the same operator is also exhausted by the same states, noting that with Eqs. (A.26) and (A.33) one has

$$m_3(Q) = \sum_{i=1}^{M} (\hbar\omega_i)^3\, |\langle i|\, Q\, |0\rangle|^2_{sc} = \frac{\hbar^4}{2m^2} \sum_{i=1}^{M} a_i^2 \tilde{C}_i \tag{A.35}$$

and with (A.18) and (A.21)—after diagonalisation—

$$\begin{aligned} \frac{1}{2}\langle 0|\, [[[\hat{H}, Q], [\hat{H}, [Q, \hat{H}]]]\, |0\rangle &= -\frac{\hbar^4}{2m^2} \sum_{i,j=1}^{M} a_i a_j \langle 0|\, [\hat{S}_i, [\hat{H}, \hat{S}_j]]\, |0\rangle \\ &= \frac{\hbar^4}{2m^2} \sum_{i=1}^{M} a_i^2 \tilde{C}_i. \end{aligned} \tag{A.36}$$

A more rigorous derivation of this generalized scaling coupled-modes approach from the HF + RPA framework is discussed in Ref. [134].

APPENDIX 2: Explicit Expressions of Operators and Sum Rules for Skyrme Forces

2.1. *The Skyrme Energy in the HF-Approximation*

The total intrinsic energy of a nucleus

$$E_{\text{tot}} = E_{\text{kin}} + E_{\text{nuc.pot.}} + E_{\text{Coul}} \tag{A.37}$$

is the sum of kinetic, nuclear potential, and Coulomb energies. For a Skyrme force in the HF approximation, the nuclear potential energy can be written [56] in terms of the local nucleon densities ($q = n, p$)

$$\rho_q(\mathbf{r}) = \sum_{i,s} |\varphi_i^q(\mathbf{r}, s)|^2 n_i^q, \tag{A.38}$$

the kinetic energy densities

$$\tau_q(\mathbf{r}) = \sum_{i,s} |\nabla\varphi_i^q(\mathbf{r}, s)|^2 n_i^q, \tag{A.39}$$

and the spin-orbit densities

$$\mathbf{J}_q(\mathbf{r}) = \sum_{i,s,s'} \varphi_i^{q*}(\mathbf{r}, s')\, \nabla\varphi_i^q(\mathbf{r}, s) \times \langle s'|\, \boldsymbol{\sigma}\, |s\rangle\, n_i^q, \tag{A.40}$$

where $\varphi_i^q(\mathbf{r}, s)$ are the single-particle wavefunctions with orbital, spin, and isospin quantum numbers i, s, and q, respectively, and n_i^q are the occupation numbers. This holds even for generalized Skyrme forces, where the density-dependent term contains a variable power σ of the density [34]. For later reference, let us add here the angular momentum densities (for spherical nuclei)

$$\lambda_q(\mathbf{r}) = \sum_{i,s} |\varphi_i^q(\mathbf{r}, s)|^2 l_i^q(l_i^q + 1) n_i^q. \tag{A.41}$$

Defining the total densities $\rho = \rho_p + \rho_n$, $\tau = \tau_p + \tau_n$, and analogously $\mathbf{J}$ and λ, let us now write down the Skyrme potential part of the total energy and introduce some names for the different terms

$$E_{\text{tot}} = E_{\text{kin}} + E_0 + E_3 + E_{\text{eff}} + E_{\text{fin}} + E_{\text{so}} + E_{\text{Coul}} \tag{A.42}$$

with

$$E_{\text{kin}} = \frac{\hbar^2}{2m} \int \tau\, d^3r, \qquad \text{(kinetic energy)}$$

$$E_0 = \frac{1}{2} t_0 \int \left[\left(1 + \frac{x_0}{2}\right)\rho^2 - \left(x_0 + \frac{1}{2}\right)(\rho_p^2 + \rho_n^2) \right] d^3r,$$

(zero-range term)

$$E_3 = \frac{1}{12} t_3 \int \rho^\sigma \left[\left(1 + \frac{x_3}{2}\right)\rho^2 - \left(x_3 + \frac{1}{2}\right)(\rho_p^2 + \rho_n^2) \right] d^3r,$$

density dependent term)

$$E_{\text{eff}} = \frac{1}{4}\int \left\{\left[t_1\left(1+\frac{x_1}{2}\right)+t_2\left(1+\frac{x_2}{2}\right)\right]\tau\rho + \left[t_2\left(x_2+\frac{1}{2}\right)-t_1\left(x_1+\frac{1}{2}\right)\right](\tau_p\rho_p+\tau_n\rho_n)\right\} d^3r,$$

(effective mass term)

$$E_{\text{fin}} = \frac{1}{16}\int \left\{\left[3t_1\left(1+\frac{x_1}{2}\right)-t_2\left(1+\frac{x_2}{2}\right)\right](\nabla\rho)^2 - \left[3t_1\left(x_1+\frac{1}{2}\right)+t_2\left(x_2+\frac{1}{2}\right)\right][(\nabla\rho_p)^2+(\nabla\rho_n)^2]\right\} d^3r,$$

(finite-range term)

$$E_{\text{so}} = \frac{1}{2} W_0 \int [\mathbf{J}\cdot\nabla\rho + \mathbf{J}_p\cdot\nabla\rho_p + \mathbf{J}_n\cdot\nabla\rho_n]\, d^3r,$$

(spin-orbit energy)

$$E_{\text{Coul}} = \frac{1}{2} e^2 \int \rho_p(\mathbf{r})\left[\int \frac{\rho_p(\mathbf{r}')}{|\mathbf{r}-\mathbf{r}'|} d^3r' - \frac{3}{2}\left(\frac{3\rho_p(\mathbf{r})}{\pi}\right)^{1/3}\right] d^3r.$$

(Coulomb energy)

The Coulomb exchange energy has, as usually, been evaluated in the Slater approximation.

In Table VIII we list the parameters of the Skyrme forces which have been used in this paper. The infinite nuclear matter properties obtained (at zero temperature) with these Skyrme forces, and referred to at various places of this paper, are given in Table IX.

TABLE VIII

Parameters of the Skyrme Forces Used in This Article

Force		SIII	SkA	SkM*	RATP
t_0	[MeVfm^3]	−1128.75	−1602.78	−2645.00	−2160.00
t_1	[MeVfm^5]	395.00	570.88	410.00	513.00
t_2	[MeVfm^5]	−95.00	−67.70	−135.00	121.00
t_3	[MeVfm$^{3+3\sigma}$]	14000.00	8000.00	15595.00	11600.00
x_0		0.45	−0.02	0.09	0.418
x_1		0.00	0.00	0.00	−0.36
x_2		0.00	0.00	0.00	−2.29
x_3		1.00	−0.286	0.00	0.586
σ		1.00	1/3	1/6	1/5
W_0	[MeVfm^5]	120.00	125.00	130.00	120.00

Note. References: SIII[129], SkA[130], SkM*[10,57], and RATP[131].

TABLE IX

Properties of Infinite Nuclear Matter, in Usual Notation, for the Skyrme Forces Used in This Article

Force		SIII	SkA	SkM*	RATP
ρ_∞	[fm^{-3}]	0.1435	0.1554	0.1603	0.1599
a_V	[MeV]	−15.857	−15.997	−15.776	−16.052
K_∞	[MeV]	355.4	263.2	216.7	239.6
J	[MeV]	28.16	32.91	30.03	29.26
m^*_∞/m		0.76	0.61	0.79	0.67
r_0	[fm]	1.180	1.154	1.142	1.143
k_F	[fm^{-1}]	1.291	1.320	1.334	1.333

2.2. *The Isoscalar Monopole Resonance* ($L=0$, $I=0$)

For the sake of completeness, we repeat here the results for the isoscalar resonance which have been derived by Bohigas *et al.* [6]. The Werntz–Überall model [29] with the single-particle excitation operator

$$\hat{Q} = \sum_{i=1}^{A} \mathbf{r}_i^2 \tag{A.43}$$

leads to a simple scaling transformation (A.7) of the single-particle wave function

$$\varphi_i^q(\mathbf{r}, \alpha) = e^{-\alpha \hat{S}} \varphi_i^q(\mathbf{r}) = e^{3\eta} \varphi_i^q(e^{2\eta}\mathbf{r}) \tag{A.44}$$

with $\eta = (\hbar^2/m)\alpha$. This gives simple expressions for the sum rules,

$$m_1 = 2\frac{\hbar^2}{m} A\langle r^2 \rangle \tag{A.45}$$

and

$$\begin{aligned} m_3 &= 2\left(\frac{\hbar^2}{m}\right)^2 [4E_{\text{kin}} + 9E_0 + 25(E_{\text{eff}} + E_{\text{fin}} + E_{\text{so}}) + 9(1+\sigma)^2 E_3 + E_{\text{Coul}}] \\ &= 2\left(\frac{\hbar^2}{m}\right)^2 A K_A^{\text{scal}}, \end{aligned} \tag{A.46}$$

where K_A^{scal} is the "scaling incompressibility" of the finite nucleus.

2.3. *The Isovector Monopole Resonance* ($L=0$, $I=1$)

In the isovector monopole case a simple ansatz for an operator which, in lowest order of a liquid drop type expansion, keeps the total density constant (i.e., contains no isoscalar contributions) is

$$\hat{Q} = \sum_{i=1}^{A} k_i r_i^2 \tag{A.47}$$

with

$$k_i = k_{q(i)} = \frac{1}{2}\left[\frac{N}{A}(1+\tau(i)) - \frac{Z}{A}(1-\tau(i))\right] = k_q \qquad (q=n,\ p) \tag{A.48}$$

with $\tau(i)$ being twice the third component of the isospin in the single-particle state $|i\rangle$,

$$\tau(i) = \langle i|\ \tau_3\ |i\rangle = \begin{cases} +1 & \text{for } q=p, \\ -1 & \text{for } q=n. \end{cases} \tag{A.49}$$

(Note that in the case $N=Z=A/2$, k_i becomes identical to $\frac{1}{2}\tau(i)$.) The scaling transformation for the single-particle wavefunctions then is

$$\varphi_i^q(\mathbf{r}, \alpha) = e^{3k_q\eta}\varphi_i^q(e^{2k_q\eta}\mathbf{r}). \tag{A.50}$$

With Eq. (A.47) the energy-weighted sum rule becomes

$$m_1 = \left(\frac{\hbar^2}{2m}\right)\frac{NZ}{2A}(\langle r_p^2\rangle + \langle r_n^2\rangle)(1+\kappa_1), \tag{A.51}$$

where κ_1 is the enhancement factor (see Eq. (2.17a))

$$\kappa_1 = \frac{1}{m_1^0}\left[\frac{A}{4}\left(\frac{1}{Z}+\frac{1}{N}\right)\right]^2\left[t_1\left(1+\frac{x_1}{2}\right)+t_2\left(1+\frac{x_2}{2}\right)\right]\int r^2\rho_p\rho_n\, d^3r. \tag{A.52}$$

There is no such simple expression for the plus-three energy-weighted sum rule like in the isoscalar case. But using Eq. (A.50), the leading term m_3^0, Eq. (2.18b) can be calculated straightforwardly by using

$$\begin{aligned}
\frac{d^n}{d\alpha^n}\rho_q\Big|_{\alpha=0} &= \{k_q[1+3(\mathbf{r}\cdot\nabla)]\}^n\rho_q, \\
\frac{d^n}{d\alpha^n}\tau_q\Big|_{\alpha=0} &= \{k_q[1+5(\mathbf{r}\cdot\nabla)]\}^n\tau_q, \\
\frac{d^n}{d\alpha^n}\mathbf{J}_q\Big|_{\alpha=0} &= \{k_q[1+4(\mathbf{r}\cdot\nabla)]\}^n\mathbf{J}_q, \\
\frac{d^n}{d\alpha^n}(\nabla\rho_q)\Big|_{\alpha=0} &= \{k_q[1+4(\mathbf{r}\cdot\nabla)]\}^n(\nabla\rho_q)
\end{aligned} \tag{A.53}$$

in evaluating the differentiations in Eq. (A.13).

2.4. *The Isovector Dipole Resonance* ($L=1$, $I=1$)

Like for all multipolarities L larger than zero, we choose for the space dependent part of the excitation operator the Tassie operator (2.20). To avoid isoscalar

contributions which would lead to a spurious center of mass motion, it is again necessary to weigh the isospin dependent part of the excitation operator with the ratios k_i (A.48) of proton and neutron numbers:

$$\hat{Q} = \sum_{i=1}^{Z} (z_i - z_{\mathrm{CM}}) = \sum_{i=1}^{A} k_i z_i. \tag{A.54}$$

This again leads to a simple form of the transformation equation (A.7),

$$\varphi_i^q(\mathbf{r}, \alpha) = \varphi_i^q(\mathbf{r} + k_q \eta \mathbf{e}_z), \tag{A.55}$$

where $\mathbf{e}_z$ is the unity vector in z-direction, and to the energy-weighted sum rule

$$m_1 = \frac{NZ}{2A}\left(\frac{\hbar^2}{m}\right)(1 + \kappa_1), \tag{A.56}$$

with the following explicit form of the enhancement factor

$$\kappa_1 = \frac{1}{2}\left[t_1\left(1 + \frac{x_1}{2}\right) + t_2\left(1 + \frac{x_2}{2}\right)\right]\frac{Am}{ZN\hbar^2}\int \rho_p \rho_n \, d^3r. \tag{A.57}$$

Evaluating the leading term of the plus-three energy-weighted sum rule Eq. (2.18b), which in the present case is just the restoring force parameter for a translational oscillation of neutrons against protons, we find

$$\begin{aligned} m_3^0 = \frac{1}{8}\left(\frac{\hbar^2}{m}\right)^2 \Bigg\{ & -\frac{4}{3} t_0\left(1 + \frac{1}{2} x_0\right) \int \nabla\rho_p \cdot \nabla\rho_n \, d^3r \\ & -\frac{1}{9} t_3\left(1 + \frac{1}{2} x_s\right)(\sigma + 2)(\sigma + 1) \int \rho^\sigma \nabla\rho_p \cdot \nabla\rho_n \, d^3r \\ & +\frac{1}{9} t_3\left(x_3 + \frac{1}{2}\right)\sigma \int \rho^{\sigma-2} \nabla\rho_p \cdot \nabla\rho_n [(\sigma - 1)(\rho_p^2 + \rho_n^2) + 2\rho^2] \, d^3r \\ & +\frac{1}{3}\left[t_1\left(1 + \frac{1}{2} x_1\right) + t_2\left(1 + \frac{1}{2} x_2\right)\right] \int (\tau_p \Delta\rho_n + \tau_n \Delta\rho_p) \, d^3r \\ & -\frac{1}{6}\left[3t_1\left(1 + \frac{1}{2} x_1\right) - t_2\left(1 + \frac{1}{2} x_2\right)\right] \int \Delta\rho_p \Delta\rho_n \, d^3r \\ & -\frac{2}{3} W_0 \int (\nabla \cdot \mathbf{J}_p \Delta\rho_n + \nabla \cdot \mathbf{J}_n \Delta\rho_p) \, d^3r \Bigg\}. \end{aligned} \tag{A.58}$$

(Note that the Coulomb and kinetic energies do not contribute to the restoring force since they are translationally invariant. In fact, the only contributions come from those terms in the total energy which include products of neutron and proton densities.)

2.5. *The Isoscalar Quadrupole Resonance* ($L=2$, $I=0$)

Like in the isoscalar monopole case we quickly review the old results of Bohigas *et al.* [6] for the isoscalar quadrupole case. With the excitation operator

$$\hat{Q}=\sum_{i=1}^{A} r_i^2 P_2(\cos\vartheta_i)=-\sum_i\left(\frac{1}{2}x_i^2+\frac{1}{2}y_i^2-z_i^2\right) \tag{A.59}$$

the transformation (A.7) reads

$$\varphi_i^q(\mathbf{r},\alpha)=\varphi_i^q(e^{-\eta}x, e^{-\eta}y, e^{2\eta}z). \tag{A.60}$$

This leads, for spherical systems, to the following expressions of the sum rules:

$$m_1=\left(\frac{\hbar^2}{m}\right)A\langle r^2\rangle \tag{A.61}$$

and

$$m_3=\left(\frac{\hbar^2}{m}\right)^2\left[4E_{\text{kin}}+4E_{\text{eff}}+4E_{\text{fin}}+E_{\text{so}}-\frac{4}{5}E_{\text{Coul}}\right]. \tag{A.62}$$

2.6. *The Isoscalar Octupole Resonance* ($L=3$, $I=0$)

The Tassie excitation operator for the isoscalar octupole resonance is

$$\hat{Q}=\sum_{i=1}^{A} r_i^3 P_3(\cos\vartheta_i)=\sum_{i=1}^{A}\left[z_i^3-\frac{3}{2}(x_i^2+y_i^2)z_i\right]. \tag{A.63}$$

Assuming spherical symmetry of the nuclear ground state, it is easy to express the energy weighted sum rule as

$$m_1=\frac{3}{2}\left(\frac{\hbar^2}{m}\right)A\langle r^4\rangle. \tag{A.64}$$

The kinetic part of the plus-three energy-weighted sum rule,

$$\begin{aligned} m_3^{\text{kin}} &= \frac{1}{2}\langle 0|\,[[\hat{H},Q],[\hat{T},[Q,\hat{H}]]]\,|0\rangle \\ &= 9\left(\frac{\hbar^2}{m}\right)^3\langle 0|-6z^2\partial_{zz}^2-3z^2(\partial_{xx}^2+\partial_{yy}^2)-\frac{3}{2}(x^2\partial_{xx}^2+y^2\partial_{yy}^2) \\ &\quad+\frac{1}{2}(y^2\partial_{xx}^2+x^2\partial_{yy}^2)-3(x^2+y^2)\partial_{zz}^2-4xy\partial_{xy}^2 \\ &\quad+6z\partial_z(x\partial_x+y\partial_y)-6z\partial_z-2(x\partial_x+y\partial_y)\,|0\rangle, \end{aligned} \tag{A.65}$$

is rather complicated to evaluate, since no closed form can be given for the scaled wavefunctions $\varphi_i^q(\mathbf{r}, \alpha)$. Even if the whole nucleus has spherical symmetry, the single-particle states with $l \neq 0$ are deformed. But assuming a nucleus with filled l-orbits—this guarantees spherical symmetry of the total density—we can average over all m_l-values

$$\langle \hat{O} \rangle_l = \frac{1}{2l+1} \sum_{m_l=-l}^{+l} \langle lm_l | \hat{O} | lm_l \rangle \tag{A.66}$$

and then easily evaluate the different terms in (A.65) in terms of three l-averaged operators

$$\begin{aligned}
\hat{\alpha}_l &= \langle z^2 \partial_{zz}^2 \rangle_l &&= \frac{1}{5} r^2 \Delta - \frac{4}{15} r \frac{\partial}{\partial r} + \frac{2}{15} l(l+1) \\
\hat{\beta}_l &= \left\langle \frac{1}{2}(x^2+y^2)\, \partial_{zz}^2 \right\rangle_l &&= \frac{1}{15} r^2 \Delta + \frac{2}{15} r \frac{\partial}{\partial r} - \frac{1}{15} l(l+1) \\
\hat{\gamma}_l &= \left\langle \frac{1}{2} z \partial_z (x \partial_x + y \partial_y) \right\rangle_l &&= \frac{1}{15} r^2 \Delta - \frac{1}{5} r \frac{\partial}{\partial r} + \frac{1}{10} l(l+1).
\end{aligned} \tag{A.67}$$

The full kinetic part of the m_3 sum rule then yields

$$\begin{aligned}
m_3^{\text{kin}} &= \frac{3}{2} \left(\frac{\hbar^2}{m} \right)^3 \left\langle -6r^2 \Delta - 12 r \frac{\partial}{\partial r} + \frac{1}{\hbar^2} \hat{l}^2 \right\rangle \\
&= \frac{3}{2} \left(\frac{\hbar^2}{m} \right)^3 \int [6r^2 \tau(r) + \lambda(r)]\, d^3r.
\end{aligned} \tag{A.68}$$

This result is quantum-mechanically exact. For application in energy density variational calculations, we need to express the angular momentum density $\lambda(r)$ through the local density $\rho(r)$. This can be done in a semiclassical density matrix expansion which is described in Appendix 3 below.

The contribution of the effective mass term, E_{eff}, in Eq. (A.42) can, after some partial integrations, be combined with the kinetic term to yield (for a spherical nucleus)

$$m_3^{\text{kin}} + m_3^{\text{eff}} = \left(\frac{\hbar^2}{m} \right)^3 3 \sum_q \int \frac{\hbar^2}{2m^*(r)} [6r^2 \tau_q(r) + \lambda_q(r)]\, d^3r, \tag{A.69}$$

where $m_q^*(r)$ is the effective mass [56]. The expression (A.69) was also derived in Refs. [132, 133].

For completeness we quote here also the finite-range and the Coulomb contributions for the octopule GR, valid for a spherical nucleus [132]:

$$m_3^{\text{fin}} = \left(\frac{\hbar^2}{m}\right)^2 \frac{9}{32}(9t_1 - 5t_2) \int r^2 \left(\frac{d\rho}{dr}\right)^2 d^3r, \tag{A.70}$$

$$m_3^{\text{Coul}} = -\left(\frac{\hbar^2}{m}\right)^2 \frac{18}{7}(4\pi e)^2 \int_0^\infty r^3 \rho_p(r)\, dr \int_0^r r'^2 \rho_p(r')\, dr'. \tag{A.71}$$

(Equation (A.70) is, strictly speaking, only correct if $\rho_n = \rho_p$, but holds within 0.1 % for the *total* m_3 for all nuclei considered here. The exact expression is easily inferred from Eqs. (A.42) and (A.70).)

APPENDIX 3: SEMICLASSICAL ANGULAR MOMENTUM DENSITY (FOR ONE KIND OF PARTICLES)

In the evaluation of E_3 for the octupole GR, we need the angular momentum density $\lambda(\mathbf{r})$, Eq. (A.41), defined in terms of the single-particle density matrix by

$$\lambda(\mathbf{r}) = \frac{1}{\hbar^2} \hat{l}_r^2 \rho(\mathbf{r}', \mathbf{r})\Big|_{\mathbf{r}=\mathbf{r}'} = \frac{1}{\hbar^2} [-i\hbar(\mathbf{r} \times \nabla_{r'})]^2 \rho(\mathbf{r}', \mathbf{r})\Big|_{\mathbf{r}=\mathbf{r}'}. \tag{A.72}$$

Using center-of-mass and relative coordinates $\mathbf{R}$, $\mathbf{s}$, we can rewrite the density matrix $\rho(\mathbf{r}', \mathbf{r}) = \rho(\mathbf{R}, \mathbf{s})$. In these coordinates the $\hat{l}_r^2$ operator yields

$$\frac{1}{\hbar^2} \hat{l}_r^2 \rho(\mathbf{r}', \mathbf{r})\Big|_{\mathbf{r}=\mathbf{r}'} = \lambda(\mathbf{R}) = -\left[\left(\mathbf{R} + \frac{\mathbf{s}}{2}\right) \times \left(\frac{1}{2}\nabla_R + \nabla_s\right)\right]^2 \rho(\mathbf{R}, \mathbf{s})\Big|_{\mathbf{s}=0}. \tag{A.73}$$

To evaluate this expression semiclassically through the local density $\rho(\mathbf{r})$, we make use of the gaussian density matrix expansion (GDME) [73] which gives to lowest order

$$\rho(\mathbf{R}, \mathbf{s}) = \rho(\mathbf{R})\, e^{-as^2}, \tag{A.74}$$

where $\rho(\mathbf{R})$ is the local single-particle density and a is chosen to yield the correct kinetic energy density τ (see Ref. [73] for details):

$$a = \frac{1}{2}\frac{\tau^*(\mathbf{R})}{3\rho(\mathbf{R})} \tag{A.75}$$

with $\tau^* = \tau - \frac{1}{4}\Delta\rho$. The angular momentum density then is easily found in terms of the local densities

$$\lambda(\mathbf{r}) = \tfrac{2}{3}r^2\tau(\mathbf{r}) - \tfrac{1}{6}r^2\Delta\rho(\mathbf{r}) + \tfrac{1}{2}\mathbf{r}\cdot\nabla\rho(\mathbf{r}), \tag{A.76}$$

and we get the semiclassical expectation value of the squared angular momentum operator after some partial integrations

$$\langle \hat{l}^2 \rangle_{\text{GDME}} = \left(\sum_i l_i(l_i+1)\right)_{\text{SC}} = \tfrac{2}{3}\int r^2\tau[\rho]\, d^3r - \tfrac{5}{2}A. \tag{A.77}$$

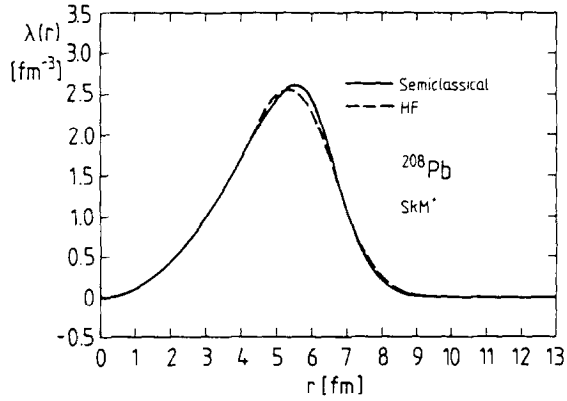

FIG. 13. Total angular momentum density $\lambda(r)$ for ^{208}Pb. Solid line: exact result (A.41), dashed line: semiclassical result (A.76) for the SkM* force.

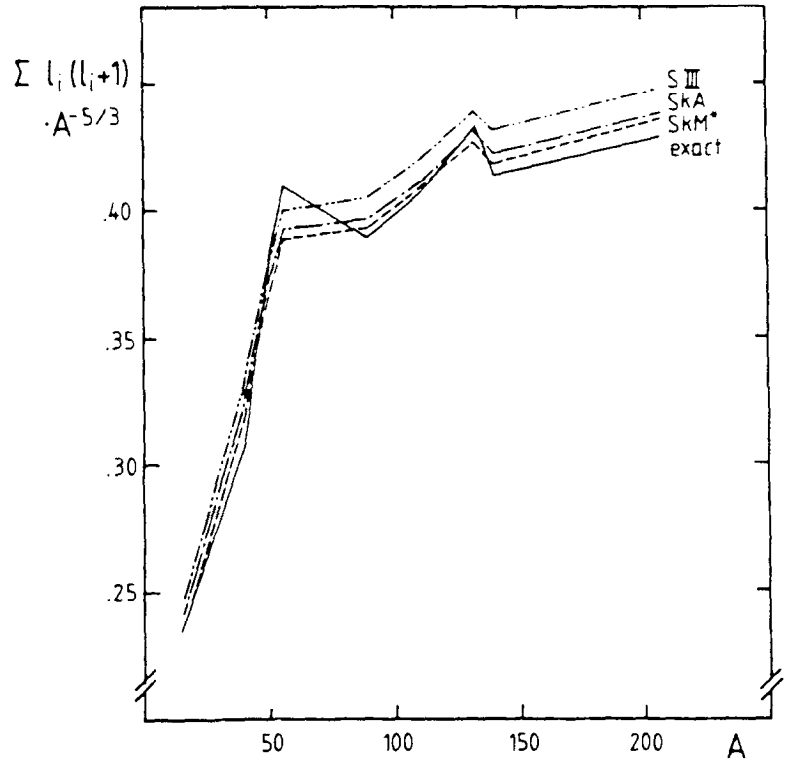

FIG. 14. Total angular momentum squared $\sum_i l_i(l_i+1)$ as a function of particle number A for some spherical nuclei. Solid line: exact values; broken lines: semiclassical values for different forces (We have calculated only the values for some spherical nuclei and connected the results with straight lines.)

In order to demonstrate the good quality of this semiclassical (GDME) approximation, we show in Fig. 13 the density $\lambda(r)$, evaluated exactly according to Eq. (A.41) and semiclassically with Eq. (A.76), for the nucleus ^{208}Pb.

The integrated squared angular momenta are shown in Fig. 14 for a series of spherical nuclei (connected by straight lines), calculated with different Skyrme forces. Note that the exact result depends on the force only through the ordering of the occupied single particle levels, which is the same here for all forces.

ACKNOWLEDGMENTS

We are grateful to M. Barranco, P. F. Bortignon, M. Buenerd, M. Casas, E. Lipparini, J. Martorell, J. M. Pearson, J. and J. P. da Providência, P. G. Reinhard, S. Stringari, and J. Treiner for many inspiring and helpful comments. We thank in particular M. Sharma for a careful reading of Section 3.1 and valuable comments on the breathing mode. We acknowledge the hospitality of all our institutions during many mutual visits. The financial support through PROCOPE has been very helpful. We also like to thank the Niels Bohr Institute, Copenhagen, for its warm hospitality towards all of us, in particular to M. B. during a sabbatical research year in which this work was completed. We thank F. Stadler who has patiently drawn all our figures. The excellent computing conditions at all institutions involved are highly acknowledged.

REFERENCES

1. G. C. BALDWIN AND G. S. KLAIBER, *Phys. Rev.* **71** (1947), 3.
2. M. GOLDHABER AND E. TELLER, *Phys. Rev.* **74** (1948), 1046.
3. H. VON STEINWEDEL AND J. H. D. JENSEN, *Z. Naturforsch. Teil A* **5** (1950), 413.
4. A. B. MIGDAL, *J. Phys. USSR* **8** (1944), 331.
5. For a review see, e.g., J. SPETH AND A. VAN DER WOUDE, *Rep. Prog. Phys.* **44** (1981), 719.
6. O. BOHIGAS, A. M. LANE, AND J. MARTORELL, *Phys. Rep.* **51** (1979), 267.
7. D. J. THOULESS, *Nucl. Phys.* **22** (1961), 78.
8. G. E. BROWN, "Facets of Physics" p. 141, Academic Press, New York, 1970.
9. E. R. MARSHALEK AND J. DA PROVIDÊNCIA, *Phys. Rev. C* **7** (1973), 2281.
10. M. BRACK, C. GUET, AND H.-B. HÅKANSSON, *Phys. Rep.* **123** (1985), 275.
11. Å. BOHR AND B. R. MOTTELSON, "Nuclear Structure," Vols. 1/2, Benjamin, Reading, MA, 1969/1975.
12. W. D. MYERS, W. J. SWIATECKI, T. KODAMA, L. J. EL-JAICK, AND E. R. HILF, *Phys. Rev. C* **15** (1977), 2032.
13. B. R. MOTTELSON, *in* "Int. Conf. on Nuclear Structure, Kingston," (D. A. Bromley and E. W. Vogt, Eds.), p. 525, Univ. Toronto Press, Toronto, 1960.
14. T. SUZUKI, *Nucl. Phys. A* **217** (1973), 182.
15. I. HAMAMOTO, Nuclear structure studies using electron scattering and photoreaction, *in* "Int. Conf. Sendai, 1972," (K. Shoda and H. Ui, Eds.), p. 205; Tohoku University Report, 1972.
16. M. GOLIN AND L. ZAMICK, *Nucl. Phys. A* **249** (1975), 320.
17. D. M. BRINK AND R. LEONARDI, *Nucl. Phys. A* **258** (1976), 285.
18. K. GOEKE, S. A. MOSZKOWSKI, AND S. KREWALD, *Phys. Lett. B* **65** (1976), 113.
19. G. F. BERTSCH, *Nucl. Phys. A* **249** (1975), 253.
20. H. SAGAWA AND G. HOLZWARTH, *Prog. Theor. Phys.* **59** (1978), 1213; G. HOLZWARTH AND G. ECKART, *Z. Phys. A* **284** (1978), 291.
21. J. P. DA PROVIDÊNCIA AND G. HOLZWARTH, *Nucl. Phys. A* **398** (1983), 59; **439** (1985), 477.

22. J. R. NIX AND A. J. SIERK, *Phys. Rev. C* **21** (1980), 396.
23. J. P. BLAIZOT, *Phys. Lett. B* **78** (1978), 367.
24. B. K. JENNINGS AND A. D. JACKSON, *Phys. Rep.* **66** (1980), 141.
25. B. K. JENNINGS, *Phys. Lett. B* **96** (1980), 1.
26. M. BRACK, *Phys. Lett. B* **123** (1983), 143.
27. L. J. TASSIE, *Aust. J. Phys.* **9** (1956), 407.
28. D. E. MEDJADI AND P. QUENTIN, *Nucl. Phys. A* **441** (1985), 294.
29. C. WERNTZ AND H. ÜBERALL, *Phys. Rev.* **149** (1966), 762; see also H. ÜBERALL, "Electron Scattering from Complex Nuclei," Academic Press, New York, 1971.
30. J. P. BLAIZOT, *Phys. Rep.* **64** (1980), 171.
31. J. MEYER, P. QUENTIN, AND B. K. JENNINGS, *Nucl. Phys. A* **385** (1982), 269.
32. K. GOEKE, A. M. LANE, AND J. MARTORELL, *Nucl. Phys. A* **296** (1978), 109.
33. D. VAUTHERIN, *Phys. Lett. B* **69** (1977), 393.
34. M. J. GIANNONI AND P. QUENTIN, *Phys. Rev. C* **21** (1980), 2076.
35. D. M. BRINK, DR. PHIL. thsis, University of Oxford, unpublished, 1955.
36. J. O. NEWTON, B. HERSKIND, R. M. DIAMOND, E. L. DINES, J. E. DRAPER, K. H. LINDENBERGER, C. SCHÜCK, S. SHIH, AND F. S. STEPHENS, *Phys. Rev. Lett.* **46** (1981), 1383; J. J. GÅRDHØJE *et al.*, *Phys. Rev. Lett.* **56** (1987), 1783; J. J. GÅRDHØJE, A. M. BRUCE, AND B. HERSKIND, *Nucl. Phys. A* **482** (1989), 121c.
37. D. H. DOWELL, G. FELDMAN, K. A. SNOVER, A. M. SANDORFI, AND M. T. COLLINS, *Phys. Rev. Lett.* **50** (1983), 1191; K. A. SNOVER, *Ann. Rev. Nucl. Part. Sci* **36** (1986), 545.
38. M. E. FABER, J. L. EGIDO, AND P. RING, *Phys. Lett. B* **127** (1983), 5; M. GALLARDO, M. DIEBEL, T. DØSSING, AND R. A. BROGLIA, *Nucl. Phys. A* **443** (1985), 415; S. ÅBERG, *Nucl. Phys. A* **473** (1987), 1.
39. M. BRACK AND P. QUENTIN, *Phys. Lett. B* **52** (1974), 159; *Phys. Scripta A* **10** (1974), 163; *Nucl. Phys. A* **351** (1981), 35.
40. U. MOSEL, P.-G. ZINT, AND K. H. PASSLER, *Nucl. Phys. A* **236** (1974), 252.
41. See, e.g., J. DES CLOIZEAUX, *in* "Many Body Physics" (C. de Witt and R. Balian, Eds.), p. 1, Gordon & Breach, New York, 1968.
42. D. VAUTHERIN AND N. VINH MAU, *Phys. Lett. B* **120** (1983), 261; *Nucl. Phys. A* **422** (1984), 140.
43. H. SAGAWA AND G. F. BERTSCH, *Phys. Lett. B* **146** (1984), 138.
44. W. BESOLD, P.-G. REINHARD, AND C. TOEPFFER, *Nucl. Phys. A* **431** (1984), 1.
45. J. BAR TOUV, *Phys. Rev. C* **32** (1985), 1369.
46. J. MEYER, P. QUENTIN, AND M. BRACK, *Phys. Lett. B* **133** (1983), 279.
47. J. MEYER, P. QUENTIN, AND M. BRACK, *in* "Proc. of the 7ème Biennale de Physique Nucléaire, Aussois, 1983," Report LYCEN 8302, p. C13-1.
48. M. BARRANCO, S. MARCOS, AND J. TREINER, *Phys. Lett. B* **143** (1984), 314.
49. M. BARRANCO, A. POLLS, S. MARCOS, J. NAVARRO, AND J. TREINER, *Phys. Lett. B* **154** (1985), 96.
50. M. BARRANCO, A. POLLS, AND J. MARTORELL, *Nucl. Phys. A* **444** (1985), 445.
51. A. S. JENSEN AND J. DAMGAARD, *Nucl. Phys A* **203** (1973), 578.
52. M. BRACK, *Phys. Rev. Lett.* **53** (1984), 119; **54** (1985), 851.
53. J. BARTEL, M. BRACK, AND M. DURAND, *Nucl. Phys. A* **445** (1985), 263.
54. M. BRACK AND J. BARTEL, *in* "Proceedings of IVth Int. Conf. on Recent Progress in Many-Body Theories, San Francisco 1985" (P. Siemens and R. Smith, Eds.), Springer-Verlag, New York, to be published.
55. T. H. R. SKYRME, *Phil. Mag.* **1** (1956), 1043; *Nucl. Phys.* **9** (1959), 615.
56. D. VAUTHERIN AND D. M. BRINK, *Phys. Rev. C* **5** (1972), 626.
57. J. BARTEL, P. QUENTIN, M. BRACK, C. GUET, AND H.-B. HÅKANSSON, *Nucl. Phys. A* **386** (1982), 79.
58. H. KRIVINE, J. TREINER, AND O. BOHIGAS, *Nucl. Phys. A* **366** (1980), 155.
59. J. DOBACZEWSKI, H. FLOCARD, AND J. TREINER, *Nucl. Phys. A* **422** (1984), 103.
60. NGUYEN VAN GIAI AND N. SAGAWA, *Nucl. Phys. A* **371** (1981), 1.

61. M. J. GIANNONI, F. MOREAU, P. QUENTIN, D. VAUTHERIN, M. VÉNÉRONI, AND D. M. BRINK, *Phys. Lett. B* **65** (1976), 305.
62. M. J. GIANNONI AND P. QUENTIN, *Phys. Rev. C* **21** (1980), 2060.
63. Å. BOHR, *Mat. Fys. Medd. Dan. Vid. Selsk.* **26**, No. 14 (1952).
64. Y. ABGRALL, B. MORAND, E. CAURIER, AND B. GRAMMATICOS, *Nucl. Phys. A* **346** (1980), 431.
65. S. STRINGARI, *Nucl. Phys. A* **279** (1977), 454.
66. S. STRINGARI, *Ann. Phys. (N.Y.)* **151** (1983), 35.
67. J. DA PROVIDÊNCIA, L. P. BRITO, AND C. DA PROVIDÊNCIA, *Nuovo Cim.* **87** (1985), 248.
68. J. P. DA PROVIDÊNCIA, Ph.D. thesis, Siegen University, 1982.
69. L. P. BRITO AND C. DA PROVIDÊNCIA, *Phys. Rev. C* **32** (1985), 2049.
70. A. S. JENSEN AND S. M. LARSEN, *Phys. Scripta* **24** (1981), 534.
71. M. BRACK AND W. STOCKER, *Nucl. Phys. A* **406** (1983), 413.
72. P. GLEISSL, M. BRACK, J. MEYER, AND P. QUENTIN, *in* "Int. Workshop on Semiclassical and Phase Space Approaches to the Dynamics of the Nucleus, Aussois 1987"; *J. Phys. (Paris) Colloq.* **48** (1987), C2-3.
73. J. MEYER, J. BARTEL, M. BRACK, P. QUENTIN, AND S. AICHER, *Phys. Lett. B* **172** (1986), 122.
74. H. M. SOMMERMANN, *Ann Phys. (N.Y.)* **151** (1983), 163.
75. R. A. BROGLIA, *in* "Lectures at the Nuclear Theory Summer Workshop," Institute of Theoretical Physics, Univ. of California, Santa Barbara, 1981.
76. H. FLOCARD, P. QUENTIN, A. K. KERMAN, AND D. VAUTHERIN, *Nucl. Phys. A* **203** (1973), 433.
77. J. TREINER AND H. KRIVINE, *Ann. Phys (N.Y.)* **170** (1986), 406.
78. A. K. DUTTA *et al.*, *Nucl. Phys. A* **458** (1986), 77; F. TONDEUR, A. K. DUTTA, J. M. PEARSON, AND R. BEHRMAN, *Nucl. Phys. A* **470** (1987), 93.
79. V. M. STRUTINSKY, *Nucl. Phys. A* **122** (1968), 1.
80. J. P. HOHENBERG AND W. KOHN, *Phys. Rev. B* **136** (1964), 864.
81. M. LEVY AND J. PERDEW, *in* "Density Functional Methods in Physics," (R. M. Dreizler and J. da Providência, Eds.), p. 11, Plenum, New York, 1985.
82. N. D. MERMIN, *Phys. Rev.* **137** (1965), A1441.
83. D. A. KIRZHNITS, *Sov. Phys. JETP* **5** (1957), 64; "Field Theoretical Methods in Many Body Systems," Pergamon, Oxford, 1967.
84. M. BRACK, B. K. JENNINGS, AND Y. H. CHU, *Phys. Lett. B* **65** (1976), 1.
85. B. GRAMMATICOS AND A. VOROS, *Ann. Phys.* **123** (1979), 359; **129** (1980), 153.
86. E. P. WIGNER, *Phys. Rev.* **40** (1932), 749; J. G. KIRKWOOD, *Phys. Rev.* **44** (1933), 31.
87. W. STOCKER, P. GLEISSL, AND M. BRACK, *Nucl. Phys. A* **471** (1987), 501.
88. C. Y. WONG AND J. A. MACDONALD, *Phys. Rev. C* **16** (1977), 1196.
89. V. M. STRUTINSKY, A. MAGNER, AND V. DENISOV, *Z. Phys. A* **315** (1984), 301.
90. A. MAGNER AND V. M. STRUTINSKY, *Z. Phys. A* **322** (1985), 633.
91. J. TREINER, H. KRIVINE, O. BOHIGAS, AND J. MARTORELL, *Nucl. Phys. A* **371** (1981), 253.
92. M. BUENERD, *in* "Int. Symp. on Highly Excited States and Nuclear Structure, Orsay 1983"; *J. Phys. (Paris), Colloq.* **45** (1984), C4-115.
93. M. M. SHARMA, W. T. A. BORGHOLS, S. BRANDENBURG, S. CRONA, A. VAN DER WOUDE, AND M. N. HARAKEH, *Phys. Rev. C* **38** (1988), 2562; M. M. Sharma, *in* "Proceedings, 26th Int. Winter Meeting on Nuclear Physics, Bormio, Italy, **N63**, 1988, p. 510.
94. J. W. S. RAYLEIGH, "Theory of Sound" p. 109 ff, Dover, New York, 1945.
95. J. D. BOWMAN, "Nuclear Structure, 1985," (R. Broglia, G. Hagemann, and B. Herskind, Eds.), p. 549, North-Holland, Amsterdam 1985.
96. M. M. SHARMA, W. STOCKER, P. GLEISSL, AND M. BRACK, *Nucl. Phys. A* (1989), in press.
97. D. GOGNY, private communication, 1983.
98. P. GLEISSL, J. MEYER, AND M. BRACK, to be published; P. GLEISSL, Ph.D. Thesis, Regensburg University, 1989 (unpublished).
99. M. B. JOHNSON, From nuclei to stars, *in* "Proceedings, Intern. School of Physics 'Enrico Fermi,' Course XCI, Varenna 1984, p. 267, North-Holland, Amsterdam, 1986.

100. D. GOGNY, *Nucl. Phys. A* **237** (1975), 399.
101. O. BOHIGAS, NGUYEN VAN GIAI, AND D. VAUTHERIN, *Phys. Lett. B* **102** (1981), 105.
102. H. KRIVINE, C. SCHMIT, AND J. TREINER, *Phys. Lett. B* **112** (1982), 281.
103. A. VEYSSIÈRE, H. BEIL, R. BERGÈRE, P. CARLOS , AND A. LEPRÊTRE, *Nucl. Phys. A* **159** (1970), 561; A. LEPRÊTRE, H. BEIL, R. BERGÈRE, P. CARLOS, J. FAGOT, A. DE MINIAC, AND A. VEYSSIÈRE, *Nucl. Phys. A* **258** (1976), 350; A. VEYSSIÈRE, H. BEIL, R. BERGÈRE, P. CARLOS, J. FAGOT, AND A. LEPRÊTRE, *Z. Phys. A* **306** (1982), 139; for reviews see also: R. BERGÈRE, Photonuclear reactions, *in* "Proceedings, Int. School on Electro- and Photonuclear Reactions, Erice, Italy, 1976" (S. Costa and C. Schaerf, Eds.), Lecture Notes in Physics, Vol. 61, Springer-Verlag, Berlin, 1977; B. L. BERMAN AND S. C. FULTZ, *Rev. Mod. Phys.* **47** (1975), 713.
104. B. L. BERMAN, R. BERGÈRE, AND P. CARLOS, *Phys. Rev. C* **26** (1982), 304.
105. J. AHRENS, H. BORCHERT, K. H. CZOCK, H. B. EPPLER, H. GIMM, H. GUNDRUM, M. KRÖNING, P. RIEHN, G. SITA RAM, A. ZIEGER, AND B. ZIEGLER, *Nucl. Phys. A* **251** (1975), 479.
106. O. BOHIGAS, Microscopic theories of nuclear collective motions, *in* "Proceedings, 5th Kyoto Summer Institute, Kyoto, July 12–16, 1982"; *Suppl. Prog. Theor. Phys.* **74, 75** (1983).
107. E. LIPPARINI AND S. STRINGARI, *Phys. Rep.* **175** (1989), 103.
108. G. J. O'KEEFE, M. N. THOMPSON, Y. I. ASSAFIRI, R. E. PYWELL, AND K. SHODA, *Nucl. Phys. A* **469** (1987), 239.
109. J. MEYER, P. QUENTIN, AND M. BRACK, *in* "Nuclear Fluid Dynamics," Proceedings, Topical Meeting on Nuclear Fluid Dynamics, Trieste, Italy, IAEA, Vienna, 1983; Report IAEA-SMR-108.
110. D. J. THOULESS AND J. G. VALATIN, *Nucl. Phys.* **31** (1962), 211.
111. D. R. INGLIS, *Phys. Rev.* **69** (1954), 1059; **103** (1956), 1796.
112. F. E. BERTRAND, *Nucl. Phys. A* **354** (1981), 129c.
113. J. R. NIX AND A. J. SIERK, *Phys. Rev. C* **21** (1980), 396.
114. F. E. BERTRAND *et al.*, *Phys. Lett. B* **103** (1981), 326; H. P. MORSCH *et al.*, *Phys. Lett. B* **119** (1982), 311.
115. P. BONCHE AND D. VAUTHERIN, *Nucl. Phys. A* **372** (1981), 496.
116. P. BONCHE, S. LEVIT, AND D. VAUTHERIN, *Nucl. Phys. A* **436** (1985), 265 and earlier references quoted therein.
117. W. STOCKER AND J. BURZLAFF, *Nucl. Phys. A* **202** (1973), 265.
118. M. BRACK, "Phase Space Approaches to Nuclear Dynamics" (M. di Toro *et al.*, Eds.), p. 417, World Scientific, Singapore, 1986; M. BRACK, "Windsurfing the Fermi Sea" (T. T. S. Kuo and J. Speth, Eds.), Vol. II, p. 219, North-Holland, Amsterdam, 1987.
119. A. BLIN AND M. BRACK, *Nucl. Phys. A* (1989), in press.
120. E. SURAUD, M. BARRANCO, AND J. TREINER, as in Ref. [72]; *J. Phys. (Paris), Colloq.* **48** (1987), C2–11.
121. W. STOCKER, *Phys. Lett. B* **142** (1984), 319; X. VINAS, M. BARRANCO, J. TREINER AND S. STRINGARI, *Astron. Astrophys.* **182** (1987), L34; C. GUET, E. STRUMBERGER, AND M. BRACK, *Phys. Lett. B* **205** (1988), 427.
122. R. C. NAYAK, J. M. PEARSON, M. FARINE, P. GLEISSL, AND M. BRACK, to be published. (Submitted to *Nucl. Phys. A*).
123. G. BAYM, H. A. BETHE AND C. J. PETHICK, *Nucl. Phys. A* **175** (1979), 225.
124. J. COOPERSTEIN AND E. BARON, Preprint BNL-42378 (1988).
125. A. L. GOODMAN, *Phys. Rev. C* **29** (1984), 1887; J. L. EGIDO *et al.*, *Phys. Lett. B* **154** (1985), 1.
126. N. D. DANG AND N. Z. THANG, *J. Phys. G (Nucl. Phys.)* **14** (1988), 1471.
127. M. BRACK, *Phys. Rev. B* **39** (1989), 3533.
128. H. FLOCARD AND D. VAUTHERIN, *Nucl. Phys. A* **264** (1976), 197.
129. M. BEINER, H. FLOCARD, NGUYEN V. GIAI, AND P. QUENTIN, *Nucl. Phys. A* **238** (1975), 29.
130. S. KÖHLER, *Nucl. Phys. A* **258** (1976), 301.
131. M. RAYET, M. ARNOULD, F. TONDEUR, AND G. PAULUS, *Astronom. Astrophys.* **116** (1982), 183.
132. M. CASAS AND J. MARTORELL, *An. Fis. (Spain)* **81** (1985), 150.
133. R. LOMBARD AND D. MAS, *Ann. Phys. (N.Y.)* **167** (1986), 2.
134. P. G. REINHARD, M. BRACK, AND H. GENZKEN, Preprint NBI, 1989, submitted to *Phys. Rev. A.*